# Observations of Particle Capture on a Cylindrical Collector: Implications for Particle Accumulation and Removal in Aquatic Systems

by

Molly R. Palmer

BS, Civil Engineering
Georgia Institute of Technology, May 2001

Submitted to the Department of Civil and Environmental Engineering in partial fulfillment of the requirements for the degree of

MASTER OF SCIENCE IN CIVIL AND ENVIRONMENTAL ENGINEERING
AT THE
MASSACHUSETTS INSTITUTE OF TECHNOLOGY

JUNE 2003



Author……
Department of Civil and Environmental Engineering
May 9, 2003

Certified By……..……..
Heidi M. Nepf
Associate Professor
Thesis Supervisor

Accepted By…….
Oral Buyukozturk
Chairman, Departmental Committee on Graduate Students

# Observations of Particle Capture on a Cylindrical Collector: Implications for Particle Accumulation and Removal in Aquatic Systems

by

Molly R. Palmer

Submitted to the Department of Civil and Environmental Engineering on May 9, 2003 in Partial Fulfillment of the Requirements for the Degree of Master of Science in Civil and Environmental Engineering

## ABSTRACT

Capture of suspended particles by cylindrical collectors is an important mechanism in many aquatic processes, such as larval settlement, suspension feeding, and vegetative filtration. The collector Reynolds number ($Re_c$), based on the collector diameter, typically ranges from 1-1000 in aquatic environments. No analytical solutions exist to describe capture efficiency in this range. Laboratory experiments are used to measure capture efficiency of a single cylinder as a function of $Re_c$ and particle ratio, $R$, which is the ratio of particle diameter to collector diameter. $Re_c$ is varied from 50 to 500 and three values of $R$ are used: 0.03, 0.015, and 0.008. For smooth cylinders, capture increases with both $Re_c$ and $R$, but is more strongly dependent on $R$. This indicates that in aquatic systems, where flow velocity and suspended particle type and size are fixed, proportionally more capture will occur on the smallest collectors (those with largest $R$). An empirical equation is developed that predicts capture to single cylinders. Furthermore, published data for an experiment in which particles are collected by branched structures can be predicted by the empirical equation. This indicates that capture to individual cylindrical branches within a compound structure can be predicted by single-cylinder efficiencies. In addition, a model of a *Spartina alterniflora* wetland is presented which shows that the mechanism of particle capture can remove a significant portion of suspended particles. Finally, experiments in which roughness elements were added to the collectors showed that capture increased when compared to the smooth cases. A model is presented based on the added drag associated with the roughness elements that describes when roughness elements can enhance, and under certain circumstances, diminish capture.

Thesis Supervisor: Heidi M. Nepf
Associate Professor of Civil and Environmental Engineering

# Acknowledgements

I thank Heidi Nepf for her constant support as an advisor, for always giving her time generously, and for being an excellent teacher. I also thank the members of my research group, Marco Ghisalberti, Anne Lightbody, Yukie Tanino, and Brian White, for being the nicest group of people I could ever ask to work with. Much thanks also to Thomas Pettersson and Joe Ackerman for their assistance and advice, especially when I was first setting up my experiments.

I owe everything to my wonderful family - my parents, Bill Palmer and Margaret Palmer, and my brother Ben Palmer - who have supported me unconditionally my whole life, and who made it possible for me to accomplish what I have. I also thank my extended family members in New England: Liz, Jon, Jim, Jen, Rob, and Shana. I am also grateful to my "godfamily", the Langshaw-Simons, for all of their love and support.

To Amie Karp, I thank her for her encouragement, laughter, and perspective. The past two years were a fated event which we will repeat again in a decade or two.

Finally, I thank Jeff Peeler for so many things it would be impossible to list them all. Very simply, I thank him for making me happy.

I also gratefully acknowledge financial support from the MIT Presidential Fellowship Program and NSF grant EAR9629259.

# Contents

# List of Figures

# List of Tables

# Notation

$b$ = equivalent upstream distance of particles that get captured on the cylinder (m)

$C$ = mass concentration (kg $m^{-3}$)

$C_D$ = drag coefficient of a smooth cylinder

$C_{Do}$= drag coefficient of a rough cylinder

$c_{sound}$ = speed of sound (m $s^{-1}$)

$D$ = diffusion coefficient ($m^2$ $s^{-1}$)

$d_c$ = cylinder diameter (m)

$d_e$ = effective diameter of a collector (m)

$d_{element}$ = average diameter of roughness element (m)

$d_p$ = particle diameter (m)

$D_{rough}$ = drag force on a rough cylinder (kg m $s^{-2}$)

$D_{smooth}$ = drag force on a smooth cylinder (kg m $s^{-2}$)

$F$ = flux of particles ($s^{-1}$)

$g$ = acceleration of gravity (9.81 m $s^{-2}$)

$h$ = water depth (m)

$k$ = settling rate constant ($s^{-1}$)

$K_C$ = particle capture rate constant for wetland model ($s^{-1}$)

$K_S$ = settling rate constant for wetland model ($s^{-1}$)

$l_c$ = collector length (m)

$l_c'$ = collector length per unit volume, $l_c/V$ (m)

$l_s$ = stopping distance of a particle (m)

$L_w$ = length of wetland (m)

$L_{50}$ = length of wetland required to reduce initial concentration by 50% (m)

$m$ = exponent in power law fit

$N_c$ = total number of particles captured to a collector over a duration $t$

$N_E$ = total number of particles capture to a roughness element over a duration $t$

$p$ = exponent in power law fit

$P$ = number concentration of particles ($m^{-3}$)

$P_0$ = initial number concentration of particles ($m^{-3}$)

$R$ = particle ratio, $d_p/d_c$

$Re_c$ = collector Reynolds number

$R_{element}$ = particle ratio of a roughness element, $d_p/d_{element}$

$s$ = specific gravity, $\rho_p / \rho_w$

$S$ = scattering strength (dB)

$S_0$ = initial scattering strength (dB)

$Stk$ = Stokes number

$Stk_{crit}$ = critical Stokes number

$t$ = time (s)

$T$ = water temperature (K)

$u$ = free stream velocity (m $s^{-1}$)

$U$ = free stream velocity (m $s^{-1}$)

v = velocity (m $s^{-1}$)

$V_p$ = volume of one particle ($m^3$)

$w_s$ = settling velocity (m $s^{-1}$)

$\delta$ = boundary layer thickness (m)

$\varepsilon$ = roughness length scale (m)

$\eta$ = total particle capture efficiency

$\eta_D$ = particle capture efficiency due to diffusional deposition

$\eta_{element}$ = capture efficiency of individual roughness element

$\eta_{num}$ = capture efficiency computed by numerical models

$\eta_R$ = particle removal due to direct interception

$\eta_{rough}$ = capture efficiency for rough collector

$\eta_{rough,SS}$ = capture efficiency for smooth areas on a rough cylinder

$\eta_{rough,RS}$ = capture efficiency for roughness elements on a rough cylinder

$\eta_{rough,100}$ = capture efficiency to the front face (front 100 degrees) of a rough cylinder

$\eta_{smooth}$ = capture efficiency for smooth collector

$\kappa$ = Boltzmann's constant ($1.38 \times 10^{-23}$ J $K^{-1}$)

$\mu$ = dynamic viscosity (kg $m^{-1}$ $s^{-1}$)

$\nu$ = kinematic viscosity ($m^2$ $s^{-1}$)

$\rho_p$ = particle density (kg $m^{-3}$)

$\rho_w$ = water density (kg $m^{-3}$)

# Chapter 1
# Introduction

Particle capture is the process by which a collector removes particles from a passing fluid. Examples of particles and their collectors are numerous: the fibers on an air conditioner filter trap airborne dust; water-borne pollen falls to the ocean floor and gets captured by a filament of algae; a silt particle is trapped by a filter in a water treatment plant. The mechanics that govern particle capture were studied first by aerosol scientists, and later by biologists and hydrodynamicists. Some analytical solutions have been derived, but very little information exists that applies to aquatic environments. Through experiments, this study investigates particle capture to cylindrical collectors in the regime of flow relevant to aquatic systems. Capture to single cylindrical collectors is observed, and results lead to an empirical equation for prediction of capture efficiency. This empirical equation is also shown to predict capture efficiency in the more complex system of branched cylinders. Finally, results from this study are used to predict how particle removal by vegetative filtration can reduce suspended sediment concentration in wetlands.

### 1.1 Literature Review

About 60 years ago, certain aerosols, or suspended airborne particles, were recognized as a threat to public health. Consequently, people became interested in how they could be removed from the air

through various filtration methods. Because scientists were interested in describing which types of filters might be better at capturing particles than others, a logical non-dimensional way to make this comparison was through a capture efficiency, $\eta$. Capture efficiency is the efficiency associated with a single cylindrical collector, and will be formally defined below. In the mid-1900's, scientists identified four mechanical processes, each with their own associated efficiencies, which make up the total efficiency, $\eta$: direct interception ($\eta_R$), inertial impaction ($\eta_I$), gravitational settling ($\eta_G$), and diffusional deposition ($\eta_D$) (Langmuir 1942; Langmuir and Blodgett 1964; Natanson 1957). The capture efficiencies are additive, such that $\eta = \eta_R + \eta_I + \eta_G + \eta_D$.

For a collector of diameter $d_c$, $\eta$ is defined as $b/d_c$, where $b$ is the upstream span of particles that are ultimately captured on the collector. As shown in Figure 1, $\eta$ represents the fraction of particles removed from the volume of water passing through the projected area of the cylinder. The relevant length scale for flow around a cylinder is the diameter, $d_c$, and flow structure is defined by the collector Reynolds number, $Re_c=ud_c/v$, where $u$ is flow velocity and $v$ is kinematic viscosity. As will be explained below, $\eta$ is a function of $Re_c$, particle specific gravity, $s$, the particle ratio $R$ (ratio of particle diameter, $d_p$, to collector diameter, $d_c$) and the Stokes number, $Stk$. Stokes number is an inertial parameter defined as the ratio of stopping distance, $l_s$, to cylinder radius. Stopping distance is the additional distance a particle would travel under its own inertia if the fluid were instantly brought to rest. Specifically, $l_s$ is a function of particle density, water density and water viscosity. However, the Stokes number is not an additional independent parameter as it can also be expressed in terms of $Re_c$, $R$, and $s$:

$$Stk = \frac{1}{9} Re_c R^2 (s-1). \tag{1.1}$$

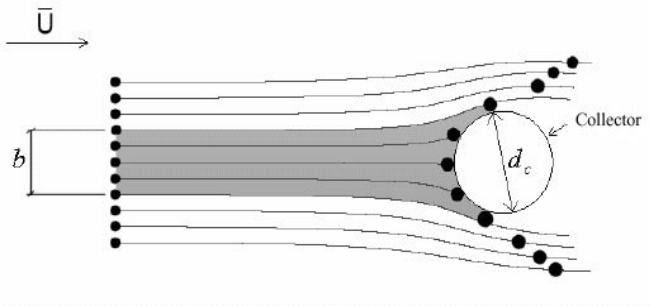


Figure 1-1. Definition of capture efficiency. Capture efficiency $\eta=b/d_c$, where $b$ is the width of particles in the flow upstream of the cylinder that will be captured, and $d_c$ is cylinder diameter. $b$ is evaluated at an upstream point at which the flow doesn't yet appreciate any effects from the cylinder.

Direct interception, $\eta_R$, describes capture due to streamline kinematics. If a particle traveling on a streamline approaches a collector within one particle radius, the particle will make contact with the collector and be captured. In 1942, Langmuir derived the equation for direct interception efficiency for creeping flow ($Re_c$<1):

$$\eta_R = \frac{1}{(2 - \ln Re_c)}\left[(1+R)\ln(1+R) - \frac{R(2+R)}{2(1+R)}\right] \qquad \text{creeping flow (1.2)}$$

In 1964, Fuchs added that if $R$<0.01,

$$\eta_R \approx \frac{R^2}{(2 - \ln Re_c)}. \qquad \text{creeping flow (1.3)}$$

For potential flow, meaning $Re_c$>1000, Fuchs (1964) shows that collection efficiency due to direct interception is:

$$\eta_R = 1 + R - \frac{1}{(1+R)} \qquad \text{potential flow (1.4)}$$

Fuchs (1964) again noted that for $R$<0.01, (1.4) can be simplified to $\eta_R \approx 2R$.

Inertial impaction occurs when a particle's inertia causes it to deviate from a streamline and collide with the collector. Aerosol theory asserts that there is a critical Stokes number, $Stk_{crit}$, below which inertial impaction is negligible. Many critical Stokes values have been suggested, ranging from

0.08 – 0.27 (Langmuir 1942; Langmuir and Blodgett 1946; Fuchs 1964). Langmuir and Blodgett (1946) suggested for potential flow that the critical Stokes value is 0.08 and:

$$\eta_I = \frac{Stk^2}{(Stk + 0.25)^2}, \quad Stk > 0.08 \qquad \text{potential flow} \quad (1.5)$$

$$\eta_I = 0 , \qquad Stk < 0.08 \qquad \text{potential flow} \quad (1.6)$$

Fuchs (1964), however, suggested that the critical Stokes value might be higher for potential flow, at about 0.125. Additionally, later studies have suggested using $\eta_I = Stk$, which is consistent with (1.5) for $Stk >> 0.25$ (Rubenstein and Koehl 1977; Shimeta and Jumars 1991).

Gravitational deposition occurs when particles settle out of the water column onto horizontal surfaces. Efficiency for this capture process has been described using equations of terminal settling velocity for a sphere. If $w_s$ is the settling velocity of a particle and $u$ is the freestream velocity, the gravitational settling efficiency for creeping flow is:

$$\eta_G = \frac{w_s}{u} = \frac{d_p^2(\rho_p - \rho)g}{u\ 18\mu}, \qquad \text{creeping flow} \quad (1.7)$$

where $\rho_p$ is the particle density, $\rho$ is the density of the fluid, $g$ is gravity, and $\mu$ is dynamic viscosity (Ranz 1951; Chen 1955; Fuchs 1964). The relevant Reynolds number for a settling particle is $Re = w_s d_p / v$. For $Re > 1$, $\eta_G$ can be computed by using appropriate equations for $w_s$ based on empirical measurements of a drag coefficient (see e.g. Streeter and Wylie 1985).

Diffusional deposition arises from any random process (i.e. Brownian motion, turbulence) that leads particles to deposit on a collector. Langmuir combined his solution for direct interception with the concept of a random walk to derive an equation for diffusional deposition efficiency. Others, including Johnstone and Roberts (1949), Ranz (1951), and Natanson (1957) suggested using a diffusion coefficient, familiar in heat and mass transfer, to describe this process. Natanson (1957) developed the following equation for diffusional deposition efficiency, $\eta_D$, for creeping flow:

$$\eta_D = \frac{1.17\pi D^{2/3}}{u d_c}\left[\frac{Re_c v}{2(2 - \ln Re_c)}\right]^{1/3}. \qquad \text{creeping flow} \quad (1.8)$$

The diffusion coefficient, $D$, is described by:

$$D = (\kappa T)/(3\pi\mu\, d_p) \tag{1.9}$$

where $\kappa$ is the Boltzmann constant, $T$ is absolute temperature, and $\mu$ is fluid viscosity (Elimelech et al. 1995).

In the 1950's and 1960's, the field of aerosol science advanced, with many reviews and books being written on the subject. Chen (1955) reviewed all the major particle capture processes and provided specific criteria for judging a filter. In 1964, Fuchs produced a volume entititled "The Mechanics of Aerosols," which was an extensive compilation of theoretical and experimental work in the field of aerosols.

In the 1970's, biologists realized that aerosol theory might help them describe aquatic particle capture processes. Rubenstein and Koehl (1977) were the first to make the case for this application. Certain organisms called suspension feeders use a process of filtration to gather food. Prior to the paper by Rubenstein and Koehl (1977), capture of particles by suspension feeders was thought to occur by sieving. That is, the food filters in the suspension feeders had a certain size "hole"; above this size, particles were trapped, and below this size, particles passed through. However, Rubenstein and Koehl suggested that the particles smaller than the "hole" size could in fact be captured to the sticky filter fibers by any one of the processes explained above. In that paper they set out to review the relevant capture processes and explain how aerosol theory might lead to quantitative biological theories in future work. Since Rubenstein and Koehl's paper, much work has been done to describe capture in aquatic systems, especially with application to suspension feeders. See the review by Shimeta and Jumars (1991) for a summary of suspension feeder particle capture theory.

Particle capture processes have been identified as important in biological processes other than suspension feeding. One such process is the recruitment of larvae in marine environments. Small particle-like larvae are transported to the beds of marine environments through a variety of mechanisms. Sometimes organisms set the path they travel through chemical or biological controls, while some organisms' paths are controlled purely by hydrodynamics. Eckman (1983) showed through experiments

that the patterns by which larvae settle onto beds depend strongly on the presence and numerical density of marsh grass stalks, suggesting that hydrodynamic particle capture to cylindrical structures is somehow important to larval recruitment. Similarly, Harvey et al. (1995) provided experimental support for hydrodynamic controls of bivalve larvae settlement onto filamentous branches of benthic algae. Finally, particle capture may be an important mechanism in the transport of submarine pollen. Indeed, Ackerman (1995) suggested pollen shape evolved in response to the physics of transport associated with flow around specific plant morphologies

Another aquatic environment in which particle capture is suspected to be important in is wetlands. The fate of suspended particles in wetlands is related to chemical fate. Because pollutants such as heavy metals tend to adsorb to suspended particles (Vaithiyanathan et al. 1993; Sansalone and Buchberger 1997), wetlands can play a role in reducing pollutant concentration. For many years, the benefits of wetlands to water quality have been known, in that they promote particle removal by enhancing residence time (Knight and Kadlec 1999) and reducing resuspension (Lopez and Garcia 1998). However, reduction in pollutant concentration due to particle capture has only recently been investigated (Reay 1972; Stumpf 1983; Jordan et al. 1986; Leonard 1995). For example, Leonard et al. (1995) observed that the capture of sediment on the stems and leaves of *Juncus roemerianus* contributed up to 10% of the total sediment deposition to a tidal marsh. Stumpf (1983) observed that 80% of the suspended material carried by flood waters disappeared within 12 m of the tidal creek, and showed that sediment found on the stems of *Spartina alterniflora* accounted for 50% of this loss. Finally, Hosokawa and Horie (1992) observed that for the same depth and flow speed the addition of artificial reeds increased particle removal by 38%. These examples suggest that physical filtration by plant structures plays some role in particle removal in aquatic systems.

### 1.2 Particle Capture Experiments

As shown in section 1.1, a wealth of literature exists to describe capture efficiency at the limits of creeping flow ($Re_c$<1) and potential flow ($Re_c$ >1000). Unfortunately, though, no theories exist in the

intermediate range of $Re_c$ =1-1000, which is the flow range of most interest in aquatic systems. Thus, in this study, laboratory experiments are used to measure capture efficiency between the limits of creeping and potential flow.

A simple cylindrical collector can be used to simulate submerged collectors. A cylindrical geometry approximates a variety of natural collectors such as: reed-like wetland vegetation (e.g. *Spartina alterniflora*, *Phragmites australis*); submerged benthic plants and algae (Harvey et al. 1995); and cilia, bristles, tube-feet and other filamentous structures of suspension feeders (Shimeta and Jumars 1991; Wildish and Kristmanson 1997; Riisgard and Larsen 2001). In aquatic systems, $Re_c$ typically ranges from 1 to 1000. Collector diameters can range in size from 1 mm (algal epibenthic collector; see e.g. Harvey et al.1995) to 2 cm (diameter of a large wetland plant stem; e.g. Hotchkiss 1972). Flow velocity $u$ ranges from 0.1 cm $s^{-1}$ to 10 cm $s^{-1}$, and particle sizes reported in the literature range from $d_p$ = 20 to 2000 $\mu$m (Shimeta and Jumars 1991). This study uses these parameters to examine particle capture on smooth and rough cylindrical collectors in a laboratory flume to better understand particle capture in aquatic systems.

Generally, prediction of $\eta$ considers only how a particle encounters a collector. In these experiments, the assumption is made that all encounters will lead to particle capture, such that encounter efficiency and capture efficiency are the same. This is a reasonable first-order assumption for aquatic plants and submerged collectors, because the sticky periphyton layer (consisting of epiphytes and organic biofilm) that grows on submerged surfaces facilitates particle retention (e.g., Borowitzka and Lethbridge 1989; Guarraci 1999). In these experiments, cylinders are coated in grease to guarantee this condition is met.

The capture efficiency defines the rate at which particles collect on a surface, which is of interest in pollination and suspension feeding, as well as the rate at which particles are removed from the water column, which is of interest in chemical fate. Consider a cylinder of length $l_c$. Let $P$ be the number concentration (# $m^{-3}$) of particles in the water. Then the flux, $F$, of particles approaching the cylinder within the region defined by the cylinder's frontal area is:

$$F = P u d_c l_c \tag{1.10}$$

The number concentration $P$ is equal to mass concentration, $C$, divided by mass of one particle (volume of one particle, $V_p$, times density of particles, $\rho_p$):

$$P = \frac{C}{V_p \rho_p} \ . \tag{1.11}$$

Recall that $\eta$ is defined as the fraction of particles approaching within the frontal area defined by (1.10) that are ultimately captured. Then the rate at which particles are captured on the cylinder (and removed from the water column) is:

$$\frac{dN_c}{dt} = \eta P u d_c l_c , \tag{1.12}$$

where $N_c$ is the number of particles captured on the collector over a given duration, $t$.

Finally, previous capture theories have only considered smooth collectors, e.g. (1.2) and (1.4) given here. However, aquatic vegetation often grows an epiphytic layer on its submerged surfaces, creating uneven surfaces that may range from micrometers to many millimeters in scale (Borowitzka and Lethbridge 1989; Wetzel 2001). In addition, many suspension feeders have roughness or protuberances on their collectors (see review in Wildish and Kristmanson 1997). Roughness elements on a collector surface can affect capture directly, by providing additional surface area, or indirectly, by altering the local flow field. Here, a preliminary assessment of the impact of roughness on capture efficiency is conducted by considering both smooth and rough cylinders.

# Chapter 2
# Experimental Methods

In this study laboratory experiments were used to observe the capture of particles by rough and smooth cylindrical surfaces over the range $Re_c$ = 50 – 500. The total capture efficiency depends only on $Re_c$ and $R$ because, for a number of reasons, direct interception is the only relevant capture process. Firstly, Stokes numbers range from $Stk = 3 \times 10^{-5}$ to $4 \times 10^{-4}$, which is significantly smaller than $Stk_{crit}$, so that the contribution to capture by inertial impaction is negligible and no dependency on specific gravity, $s$, is considered. In addition, the vertical orientation of the collector precluded gravitational deposition. While there is no analytical expression for diffusional deposition at $Re_c$ =50-500, $\eta_D$ can be estimated for creeping flow from (1.8). Since $\eta_D$ is inversely proportional to $u$, this estimate is an upper bound for $\eta_D$ in our experiments. From (1.8) and (1.9) at $Re_c$ = 0.1, diffusional deposition efficiency for the particle and collector sizes used is on the order of 0.001%. This is an order of magnitude smaller than the capture efficiencies observed, order 0.01% or greater. Consequently particle capture due to diffusion is expected to be negligible in this study.

Capture efficiency is measured by allowing particles to collect on a cylinder for duration $t$. By counting the number of particles collected, $N_c$, one can estimate $dN_c/dt$ and then infer $\eta$ from (1.12). With $s$=1.03, $P$ decreased significantly over the duration of the experiments due to settling of particles onto the channel bed. $P(t)$ is estimated by writing an expression for the flux of particles to the bed:

$$\frac{\partial P}{\partial t} = \frac{-w_s}{h} P \tag{2.1}$$

where $w_s$ is the settling velocity of the particles (or Stokes' velocity) and $h$ is height of water in the flume. The decay given in (2.1) assumes that turbulence in the water and mixing produced by the pumps keeps the concentration in the water column uniform over depth. This assumption is later confirmed by continuous measurements of concentration, which decay exponentially as implied by (2.1). The quantity $w_s/h$ is replaced by the constant $k$, henceforth referred to as the settling rate constant, and (2.1) is integrated to derive an expression for concentration decay with time, $t$:

$$P(t) = P_0 e^{-kt} . \tag{2.2}$$

Incorporating (2.2) into (1.12) and integrating gives the expression used to estimate capture efficiency accounting for settling loss:

$$\eta = \frac{N_c k}{P_0 u d_c l_c (1 - e^{-kt})} . \tag{2.3}$$

This assumes capture begins at $t$=0 and ends at time $t$. $P_0$ is the number concentration of particles when the cylinder is inserted.

**2.1 Flume and Flow Characteristics**

Experiments were conducted in a flume 2.75 m long, 22 cm wide, and 20 cm high. Water depth, $h$, ranged from 9.0 to 10.5 cm varying with the Reynolds number desired for each experiment. A recirculating flow was generated using up to three different pumps, which included a small centrifugal pump (Micropump, model 101-000), and two peristaltic pumps (Manostat Varistaltic Power Pump model 72-370-000). At the inlet, water was pumped via tubing into a stilling basin and then passed through four aluminum screens (hole diameter 6.35 mm, 57% open area) to straighten the flow, as is shown in Figure 2-2A.

Velocity profiles were measured with an acoustic Doppler velocimeter (ADV, SonTek 10 MHz) and visualized with dye at multiple longitudinal positions (see section 2.3 for details on ADV operation).

Based on these profiles and the criteria given below, the longitudinal location 2 m downstream of the inlet was chosen for the cylinder test position. The flow was examined in the lateral and vertical directions to determine the size of the boundary layers and of the central region of uniform flow. At $x$ = 2 m the lateral profile was not fully developed, with the boundary layers extending less than 4 cm from the two side walls. The middle 14 cm of the flow was laterally uniform. Vertically, the bottom boundary layer extended less than 4 cm. Above this, the velocity exhibited no more than 10% variation. Thus a test section of uniform flow is defined between $z$ = 4 cm and the surface. The collector area (see Figure 2B) was fully inside this region. The Reynolds number calculated for each trial was based on the average flow velocity from $z$ = 4 to $z = h$. Specifically, three flow rates were used to achieve three average flow velocities (0.6 cm $s^{-1}$, 1.0 cm $s^{-1}$, and 1.8 cm $s^{-1}$) over the range of $z$ = 4 to $z = h$, as shown in Figure 2-2. Additionally, velocity profiles and dye visualizations indicated that at a longitudinal position of $x$ = 2m, the suction condition at the outlet did not affect the flow in either the lateral or vertical directions.

**2.2 Particles**

An industrial plastic resin (Eliokem Pliolite VTAC-L, $s$=1.03) was chosen for the experimental particles, for its relatively low density, its white color, and the round shape of its particles. The resin was sieved on a shaker table using US standard sieves #70 and #80, having opening diameters of 210 μm and 177 μm, respectively. The fraction captured between these two sieves was used for the experiments; thus the average particle size was estimated as 194 μm ± 17 μm.

12.0 g of sieved Pliolite, measured on a scale (Ohaus model TS400s, readability 0.01 g), was put into suspension using a small amount of surfactant. The suspension was then poured into the flume, which was stirred until the particles spread out over the length of the flume. Since the water recirculated, the same mass of particles could be reused for multiple trials, as removal due to particle capture provided an insignificant reduction in particle concentration (a typical cylinder collected about 50-200 particles per experiment, much less than the millions of particles present in the flume).

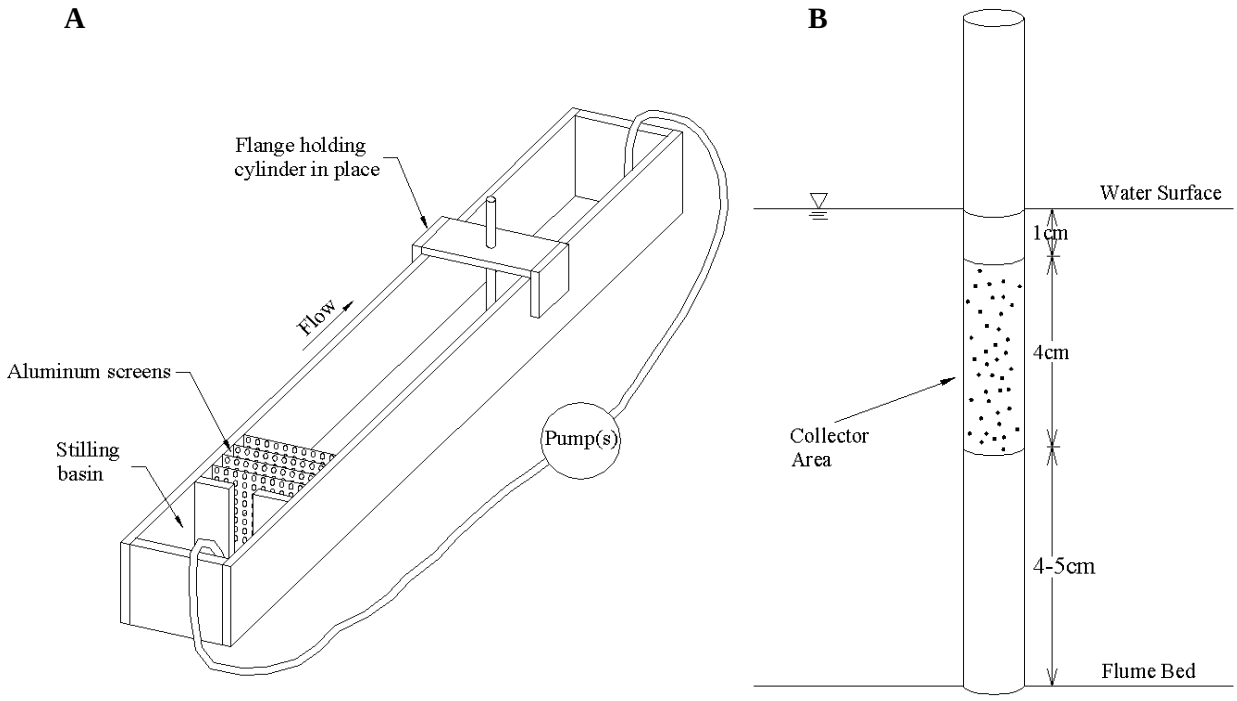


Figure 2-1. Flume setup and cylinder dimensions. (A) In the recirculating flume, water is pumped into a stilling basin and then through a set of four aluminum screens that straighten the flow. The cylinder is held in place from above by a flange at a distance of 2 meters from the inlet. (B) The collector area on the cylinder is a 4 cm-long section located 1 cm below the surface of the water.

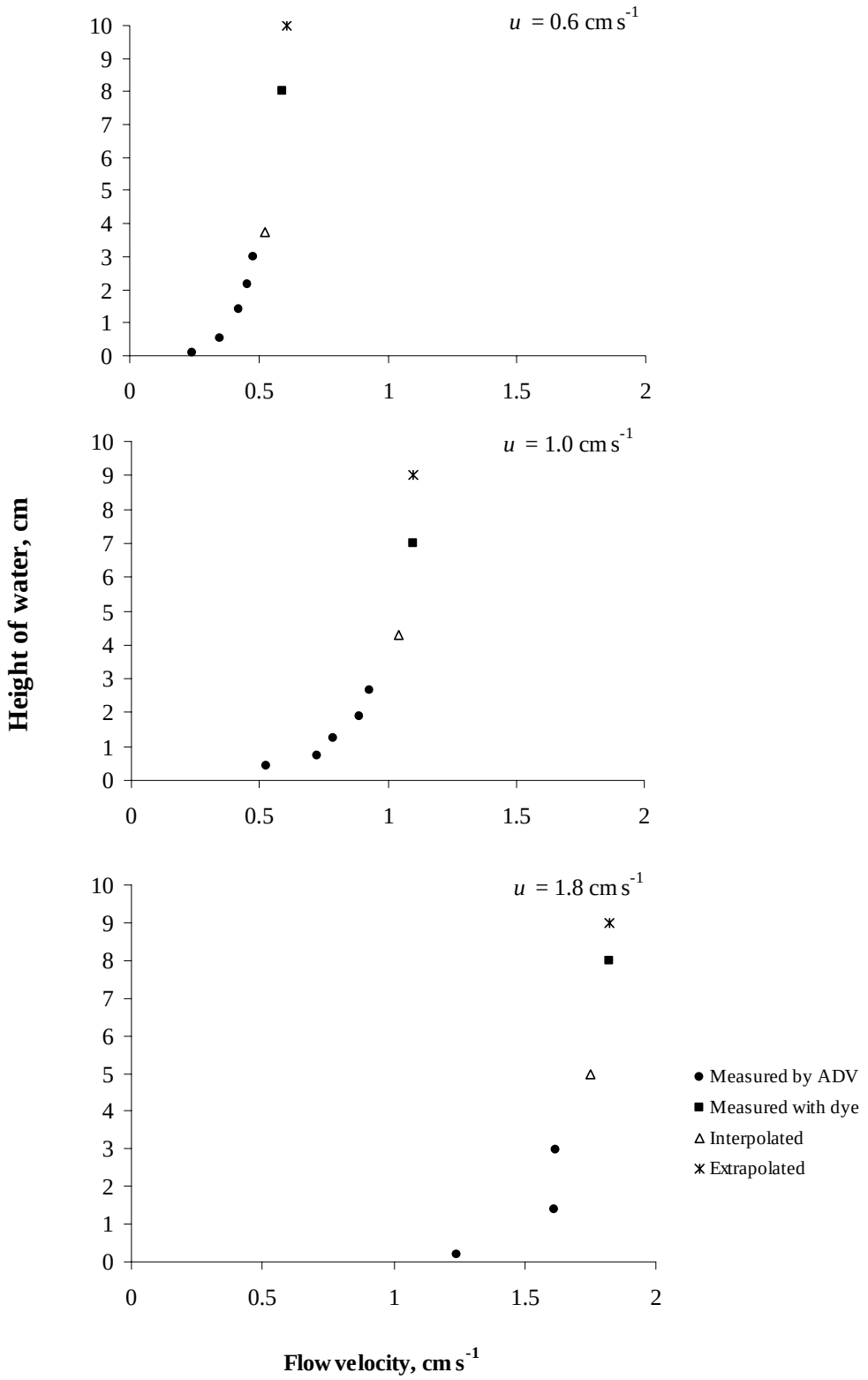


Figure 2-2. Vertical profiles of velocity at cylinder test section for three flow rates used. The ADV was used to measure velocities from z = 0 to z = 3 cm. However, due to the shallow water in the flume, it could not be used at heights above 3 cm. Instead, dye traces were used to measure velocity in the upper region of the flow and points were interpolated and extrapolated from the combined measurements.

## 2.3 ADV

As discussed in section 2.1, an ADV was used to measure flow velocity in the flume. In addition, it was used to monitor particle concentration in the flume. Methods for using the ADV for both of these applications are discussed below.

### 2.3.1 Measuring Velocity

The ADV operates by the principle of Doppler shift. This concept is illustrated by a simple example: if an ambulance passes by you while you're standing on the street, you hear the siren at a higher pitch as the ambulance approaches, and then a lower pitch as it leaves. As the ambulance moves toward you, sound waves from the siren are compressed (meaning higher frequency) and you perceive the sound at a higher pitch. As the ambulance leaves you, sound waves are no longer compressed and you hear a lower-pitched, lower frequency noise. This shift in frequency can be calculated using the equation:

$$F_{dopper} = -F_{source}\frac{\mathrm{v}}{c_{sound}} \tag{2.4}$$

where $F_{doppler}$ is the change in received frequency (Doppler shift); $F_{source}$ is the frequency of transmitted sound; v is velocity of the source relative to receiver; and $c_{sound}$ is the speed of sound. For there to be a Doppler shift, there must be relative motion between the sound and the observer; if you were in the ambulance and moving with it, you would hear the siren at one pitch for the entire trip. This is evidenced in the equation – if relative velocity between the sound and observer is zero (v=0), there is zero shift of frequency.

The ADV uses this principle to measure the velocity of water in three dimensions. The device sends out a beam of acoustic waves at a fixed frequency from a transmitter probe. These waves bounce off of moving particulate matter in the water and three receiving probes "listen" for the change in frequency of the returned waves. The ADV then calculates the velocity of the water in the *x*, *y*, and *z* directions. A general schematic of the ADV is shown in Figure 2-3.

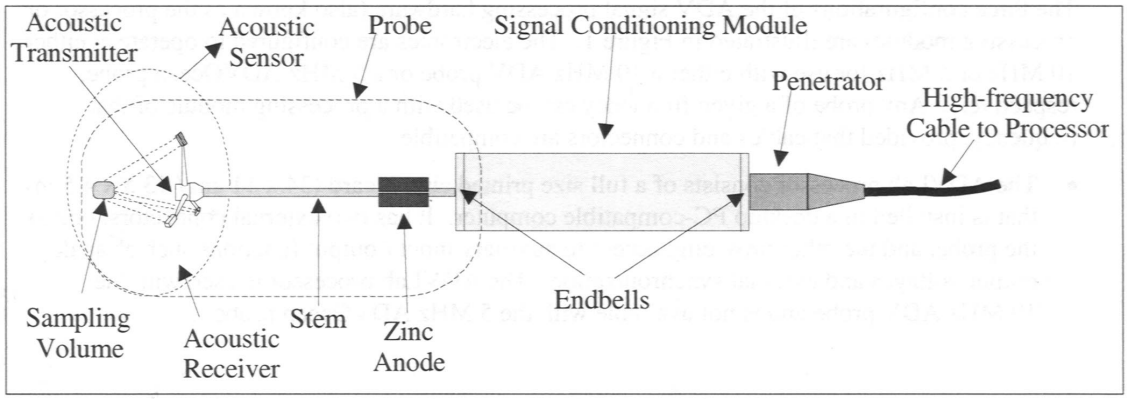

Figure 2-3. Schematic of Sontek ADV Probe (from Sontek 1997).

*Seeding the flow* – As explained above, the ADV sends out acoustic waves that must bounce off of particulate matter in the flow. In the field, water is often dirty enough that adding particles is not necessary (or practical). In the lab, however, water is usually quite clean and requires artificial introduction of particles. This is called seeding. The minimum particle size that Sontek (an ADV manufacturer) recommends is 2 μm. Thus, particles larger than this size that remain in suspension in the water can be used as seeding material. To check if water is properly seeded, the Sontek ADV software interface provides a signal-to-noise ratio (SNR). This is an indicator of how well the flow is seeded: the higher the SNR, the better the seeding and the more reliable the velocity measurements. In the laboratory, the minimum SNR at which the ADV should be operated is about 15.

*Positioning the ADV* – Four acoustic probe tips (one transmitter and three receivers, shown in Figure 2-4) all send and receive acoustic information in a fluid volume below the ADV, referred to as the sampling volume. Because the ADV is inserted into the flow, the sampling volume must be far enough away from the probe tip so as not to disturb the flow and the velocity measurements. Thus, it is located about 7 cm below the probe tip. When positioning the ADV near boundaries, the user must be particularly aware of the sampling volume location.

The Sontek ADV software program allows the user to easily check if the sampling volume is too close to the boundary. Using acoustic waves, the ADV directly measures how far away the probe tip and sampling volume are from the bottom boundary. The program displays this in real-time so the user can make adjustments if there are any conflicts. This is also a reliable way to find the z-coordinate of the sample volume.

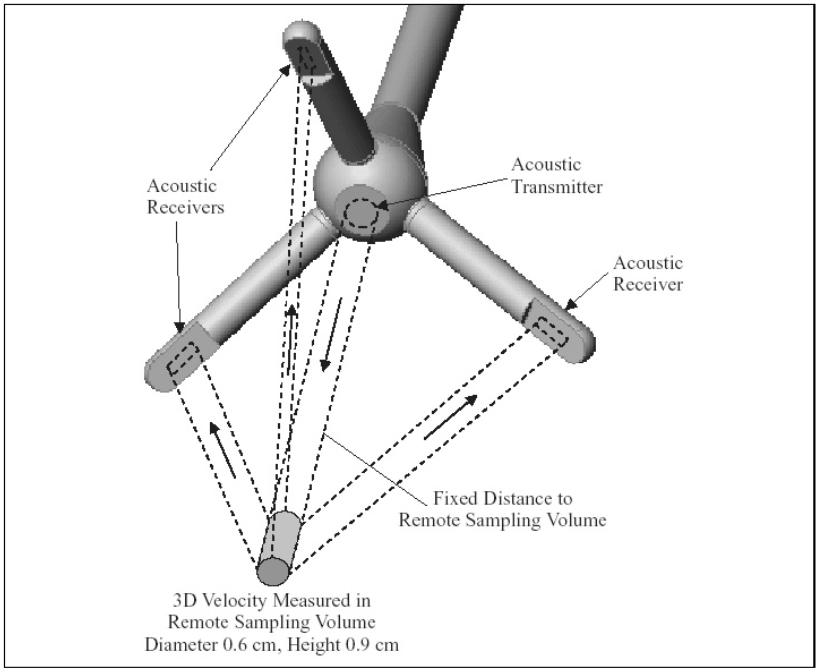


Figure 2-4. Schematic of ADV probe tip and sampling volume. The distance from the transmitter to the sampling volume in the 10 MHz SonTek ADV is about 7 cm. (from SonTek)

*Setting parameters* – Once the flow is seeded and the ADV positioned, certain parameters about the laboratory setup must be configured in the ADV software:

- Sampling rate: The user sets the sampling rate, which is how often the ADV collects data. The range for this is 0.1-25 samples per second (Hz). Usually, using 25 Hz is the most appropriate value, since it provides the highest temporal resolution.

- Temperature and Salinity: The speed of sound is a function of both temperature and salinity. Accordingly, it is important that the user measure these values accurately to better tune velocity measurements.
- Maximum velocity range: The selectable values of maximum velocity range from 3 cm $s^{-1}$ to 250 cm $s^{-1}$. The user should select the lowest value that adequately encompasses the velocity range. For example, if one expects the measured velocities to be in the range of 4-8 cm $s^{-1}$, the appropriate maximum velocity would be 10 cm $s^{-1}$. Selecting 100 cm $s^{-1}$ would unnecessarily decrease the instrument resolution and thus the accuracy.

*Uncertainty* – As with all measurements, there is some uncertainty associated with velocities measured by the ADV. One primary source of bias comes from inputting salinity and temperature. If these are not accurately measured, or if conditions change while the experiment is being run, the velocity measurements will be biased.

Another source of uncertainty is Doppler noise, which SonTek states is an artifact of acoustic scattering and can be assumed to be purely random. At a sampling rate of 25Hz and an SNR above 15, uncertainty due to Doppler noise can be estimated as 1% of the maximum velocity range.

To evaluate quality of velocity measurements, one of the real-time outputs the ADV provides is a correlation statistic. This is a value ranging from 0% - 100%. The closer the correlation is to 100%, the less noisy and more reliable a velocity measurement is. SonTek recommends 70% as the minimum acceptable correlation. This correlation, when used with SNR, provides an excellent way to gauge the quality of the ADV measurements.

In these experiments, velocity records were taken at 25Hz for a minimum of five minutes. The value reported was the average value of velocity over the record duration. The Pliolite particles acted as a very good seeding material, so no additional seeding was necessary. SNR and correlation were relatively high: generally, SNR ranged from 15 to 30, and correlation was always above 90%. Thus, velocity measurements had small uncertainties.

### 2.3.2 Monitoring Concentration

Although primarily used to measure flow velocity, an ADV can be used to monitor concentration of suspended particles in water. For these experiments, the ADV was used to find the settling rate constant, *k*, for use in (2.3). To measure velocity, a flow must be seeded with suspended particles so that acoustic waves can bounce off of them. In the process of determining flow velocity, the ADV also tracks information on the backscatter caused by seeded particles. This backscatter, or scattering strength, is what permits the ADV to be used for the secondary purpose of measuring concentration.

SonTek states, "At a single frequency, scattering strength is a function of the particle type, size, and concentration" (1997). If particle type and size distributions are constant, scattering strength is directly proportional to concentration. In a laboratory setting, then, where suspended particles in a flow are of consistent size, relative differences in concentration are determined by comparing measured signal levels. Absolute measurement of concentration requires the additional step of calibration.

A record of scattering strength is automatically recorded by the ADV when a velocity record is taken (in fact, records can be used to simultaneously monitor scattering strength and velocity). Thus, the ADV is set up and configured as if velocity measurements were being taken.

An important factor in getting good concentration measurements is choosing appropriate particles. They must be of a consistent size distribution. The size distribution will often be known, but this is not always necessary – one simply must be confidant that the size distribution will be uniform from sample to sample. Particles also must be large enough to be detected by the probe. The SonTek ADV probes used in the Parsons Lab operate at 10 MHz and measure a minimum particle size of 2 μm in diameter. (Note: other SonTek probes, such as microADV and ADVOcean, or probes made by other manufacturers, may operate at different frequencies and have different detection limits). The 200-μm Pliolite particles used in these experiments were of a known particle size distribution and were well above the detection limit.

The ADV outputs scattering strength in units of counts; however, these should be converted to decibels. SonTek states that for their probes, 1 count is equal to 0.43 decibels (Although linear here, the

relationship of a count to a decibel is not always so). Since decibels are on a logarithmic scale, a difference in signal level is converted to a linear ratio of concentrations by:

$$S - S_0 = 10\log\left(\frac{P}{P_0}\right), \tag{2.5}$$

where $S$ is the scattering strength in dB, $S_0$ is the initial scattering strength in dB, and $(P/P_0)$ is the ratio of the concentration to initial concentration. The factor of 10 in (2.5) arises because 1 Bel = 10 dB. Thus by measuring $S(t)$, one can describe how concentration, P, decays with time.

### 2.3.3 Computing settling rate constant

The relationship of signal strength to measured concentration given by (2.5) can be combined with (2.2), the exponentional settling model, to get:

$$S - S_0 = 10\log\left(e^{-kt}\right), \tag{2.6}$$

which reduces to a linear equation having the form:

$$S = [S_0] - [10k\log(e)]t\,. \tag{2.7}$$

The settling rate constant, $k$, is found by fitting observed scattering strength measurements to (2.7).

Scattering strength and particle capture efficiency were not measured simultaneously because the presence of the ADV probe tip in the water was disruptive to the flow. Instead, two replicate concentration records were measured prior to each set of capture experiments. Procedures for taking a concentration record and performing a particle capture trial were identical, the only difference being the presence of the ADV probe tip or the collector cylinder. Because of this, the concentration measurements taken prior to each experiment set were indicative of the settling rates in the particle capture trials. To ensure that all particles settled out of the flume, each ADV record lasted 40 minutes. However, since experiment durations were 400 – 600 s, a linear fit was only applied to the first 1000 seconds of the ADV record. The sampling rate of each record was 10 Hz. Three typical records of scattering strength vs. time are shown in Figure 2-5.

For each scattering strength record, a linear regression based on 12,000 points gave an *r*-squared correlation of greater than 0.57. Standard errors associated with calculating the intercept and slope of the line were always <1%, so uncertainty in calculating *k* was very low. Based on (3.14), the slope *m* of the linear regression yields the settling rate $k=m/(10\log(e))$. Throughout the experiments *k* was not constant due to a decreasing settling velocity, $w_s$, associated with the Pliolite particles. Over time, Pliolite was observed to very gradually absorb water, decreasing its density and therefore its settling velocity. For example, over the duration of the smooth experiments, the settling velocity decreased from about 0.05 cm $s^{-1}$ to 0.03 cm $s^{-1}$.

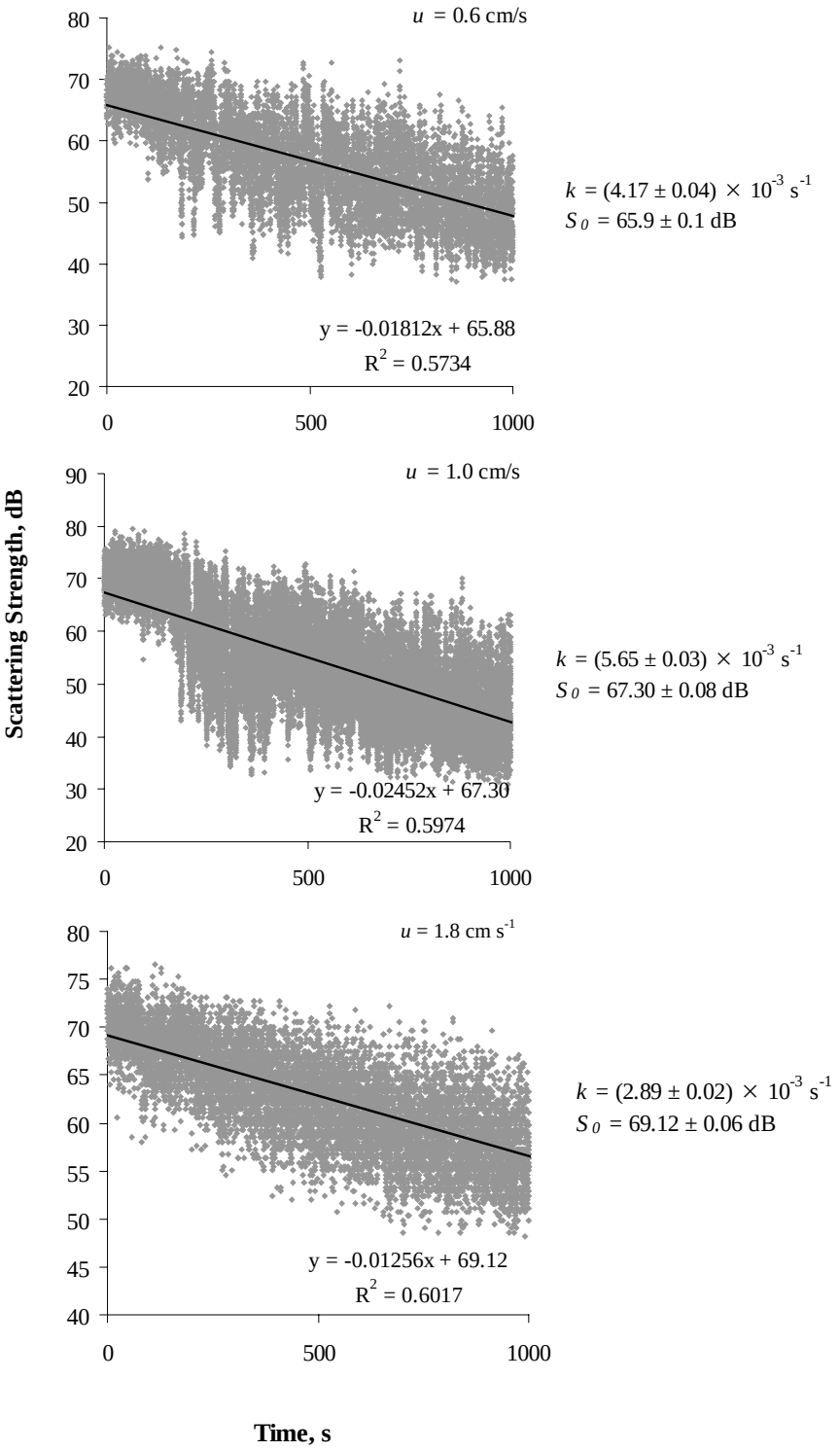


Figure 2-5. Sample ADV scattering strength records. Figure 3. Sample ADV record of scattering strength over the duration of an experiment. ADV samples points ( ◆ ) were taken at a rate of 10 $s^{-1}$. Solid lines represent linear fits to the equation of the form $S=S_0-mt$. The settling rate constant, $k$ equals $m/[10\log(e)]$. Values of $k$ and $S_0$ are indicated to the right of each graph.

## 2.4 Smooth Experiments

Three different size plastic cylinders (Delrin®, DuPont Engineering Polymers) of diameters 0.635 cm, 1.27 cm, and 2.54 cm were used as smooth collectors. The manufacturer's tolerance on the Delrin rods is 0.005 cm, and any variation in size of the cylinders was negligible. Three different flow rates were used, yielding a total of nine different collector Reynolds numbers, ranging from 50 to 500, and three different $R$ ratios (0.008, 0.016, and 0.03).

Cylinders were prepared by marking off a four-centimeter-long test section. In this section the black Delrin® was left exposed so that the white Pliolite particles would be clearly visible. The rest of the cylinder was covered in white tape. The front of the cylinder, which points directly upstream, was marked with a vertical red line, indicating the zero-degree mark. The cylinder was greased by applying a liberal coating, about 2-3 mm thick, of clear silicone grease (Chemplex silicone compound 710 by NFO Technologies). The excess grease was then wiped off with a paper towel in one pass, leaving a thin, uniform coating of negligible thickness ($<<1$ mm). An end-on visualization confirms that the thickness is uniform around the cylinder and is not thick enough to significantly change the diameter of the cylinder. This process was quite repeatable such that the grease layer thickness was constant from trial to trial.

The flume was stirred by hand for about one minute to bring it to fully-mixed conditions. Because flow was very turbulent from the mixing, it was allowed to straighten out for 60 s before the cylinder was lowered into the flume. When inserted in the water, the 4-cm test section began one centimeter below the surface of the water so that surface effects were minimized (see cylinder orientation in Figure 2-2B). The red line at the zero-degree mark was aligned with the upstream, and particles were allowed to collect for a duration ranging from 6 to 10 minutes, depending on how much time was needed for a significant number of particles to collect.

The cylinder was removed at the end of the experiment and allowed to dry. It was then photographed with a 4.1-megapixel digital camera (Sony DSC-S85 Cyber-shot®). Although Pliolite particles are visible to the naked eye and could be counted by hand, taking a digital photo the view of the cylinder to be magnified while collecting photos for future reference. For the smooth experiments, one

photo taken from the front was sufficient to photograph almost all the captured particles because capture was limited to ± 50 degrees from the front. During some of the higher Reynolds number experiments, a small number of particles deposited on the back side of the cylinder. These were simply counted by hand, as there were usually fewer than 10.

### 2.5 Rough Experiments

The procedure for the rough experiments was the same as for the smooth, except roughness elements were added during the greasing process. Instead of roughening the surface of the cylinder and then greasing it, a more uniform and consistent roughness was produced using the grease itself to create roughness elements. These elements retained their shape when inserted into flowing water. A flat nail head was used to apply a dot of grease to the cylinder. The nail head was then pulled away from the cylinder, bringing the grease out to a point and forming a nearly conically shaped roughness element, shown in Figure 2-5A. The diameter at the base of these roughness elements was about 1.5 mm, and the elements protruded a distance of 1.5-2 mm. This scale of roughness was chosen because it was significantly larger than the particle size and also larger than the estimated boundary layer thickness. Based on numerical calculations (reported in Pettersson et al. In Prep), for the range of $Re_c$ used in the rough experiments, the boundary layer thickness, $\delta$, varied from 0.6 mm to 1.5 mm, depending on the radial position around the cylinder and the Reynolds number.

The roughness elements were placed on the cylinder in two array patterns. Initially, two sets of experiments were conducted using a low-density configuration: this consisted of 8 staggered rows (a row every 45 degrees) around the cylinder, with a total of 60 elements and a density of about 4 elements per $cm^2$, as shown in Figure 2-5B. One experiment set was also conducted at a higher-density roughness pattern of 8 elements per $cm^2$. This pattern was made up of 12 rows (a row every 15 degrees) in an unstaggered pattern, as shown in Figure 2-5C.

With roughness, particle deposition was more spread out than with smooth cylinders, so photographs were taken covering the full 360 degrees of the rough cylinders. During counting a

distinction was made between particles that deposited on a roughness element and those that deposited on a smooth area of the cylinder, and detailed information on the spatial distribution of particles was collected.

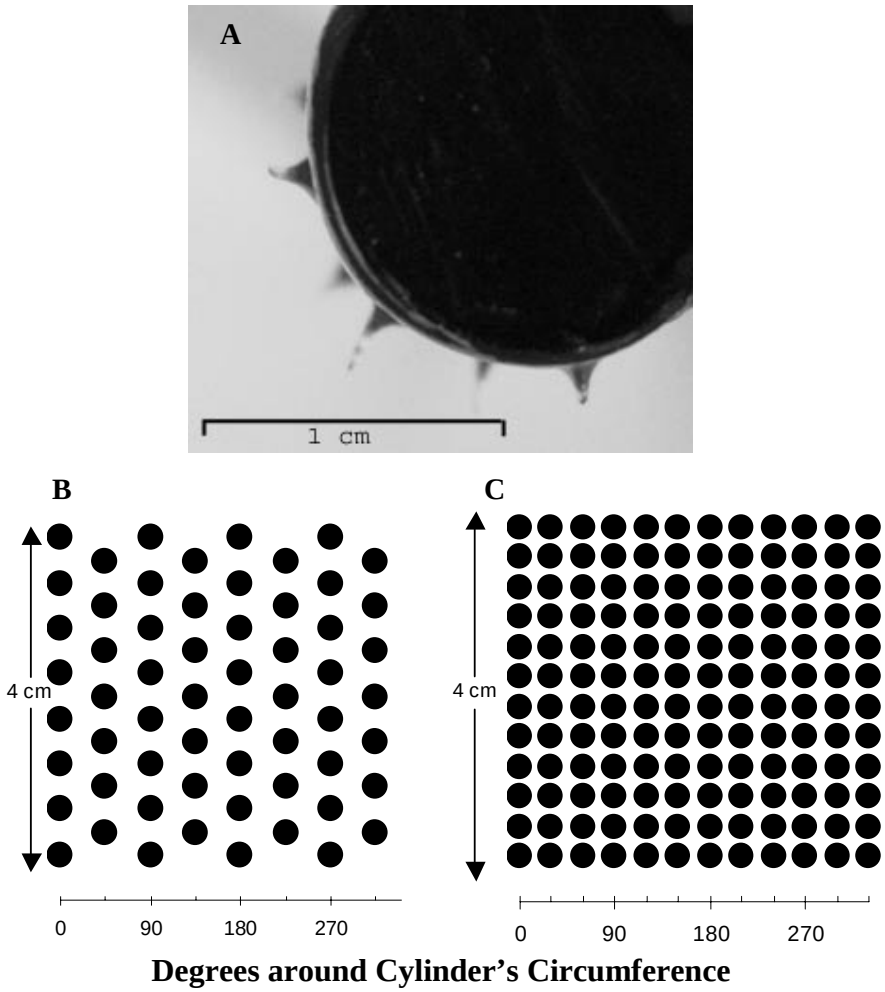


Figure 2-5. Geometry and placement of roughness elements. (A) Cross-sectional view of roughness elements. Applying a small dot of grease to the cylinder and pulling the nail head outward created the conically-shaped elements. The resulting element shape has a base diameter of about 1.5 mm and a protruding length of 1.5 – 2 mm. (B) 'Unrolled' arrangement of roughness elements on the collector area in low-density configuration (4 $cm^{-2}$). The rows are staggered for a total of 60 elements per cylinder. (C) Similar 'unrolled' arrangement for high-density configuration (8 $cm^{-2}$). Here, the rows are not staggered.

Table 2-1. Parameters for Smooth Experiments

| Date | Experiment Set | Number of Trials | Cylinder Diameter, $d_c$ | Particle Diameter, $d_p$ | Average Velocity, $u$ | Height of Water, $h_w$ | Settling Rate Constant, $k$ | Initial Particle Concentration, $P_0$ | Duration of experiment, $t$ | Average Water Temperature, $T_w$ | Kinematic Viscosity, $\nu$ | Reynolds Number, $Re_c$ | Particle Ratio, $R$ |
|---|---|---|---|---|---|---|---|---|---|---|---|---|---|
| | | | [m] | [m] | [m $s^{-1}$] | [m] | [$s^{-1}$] | [# $m^{-3}$] | [s] | [C] | [$m^2$ $s^{-1}$] | -- | -- |
| 20-Jun-02 | 1 | 5 | 0.00635 | 1.94E-04 | 0.010 | 0.090 | 0.0056 | 6.0E+07 | 360 | 22.0 | 9.33E-07 | 68 | 0.031 |
| 20-Jun-02 | 2 | 5 | 0.0127 | 1.94E-04 | 0.010 | 0.090 | 0.0056 | 6.0E+07 | 480 | 22.3 | 9.26E-07 | 137 | 0.015 |
| 20-Jun-02 | 3 | 5 | 0.0254 | 1.94E-04 | 0.010 | 0.090 | 0.0056 | 6.0E+07 | 600 | 23.0 | 9.09E-07 | 279 | 0.008 |
| 11-Jul-02 | 4 | 5 | 0.00635 | 1.94E-04 | 0.006 | 0.100 | 0.0042 | 5.4E+07 | 360 | 18.8 | 1.01E-06 | 38 | 0.031 |
| 11-Jul-02 | 5 | 5 | 0.0127 | 1.94E-04 | 0.006 | 0.100 | 0.0042 | 5.4E+07 | 480 | 18.8 | 1.01E-06 | 76 | 0.015 |
| 12-Jul-02 | 6 | 5 | 0.0254 | 1.94E-04 | 0.006 | 0.100 | 0.0042 | 5.4E+07 | 600 | 18.3 | 1.02E-06 | 149 | 0.008 |
| 12-Sep-02 | 7 | 5 | 0.00635 | 1.94E-04 | 0.018 | 0.095 | 0.0028 | 5.4E+07 | 360 | 19.3 | 9.96E-07 | 115 | 0.031 |
| 12-Sep-02 | 8 | 5 | 0.0127 | 1.94E-04 | 0.018 | 0.095 | 0.0028 | 5.4E+07 | 480 | 21.0 | 9.56E-07 | 239 | 0.015 |
| 12-Sep-02 | 9 | 5 | 0.0254 | 1.94E-04 | 0.018 | 0.095 | 0.0028 | 5.4E+07 | 600 | 21.7 | 9.40E-07 | 486 | 0.008 |



Table 2-2. Parameters for Rough Experiments

| Date | Experiment Set | Number of Trials | Cylinder Diameter, $d_c$ | Particle Diameter, $d_p$ | Average Velocity, $u$ | Height of Water, $h_w$ | Settling Rate Constant, $k$ | Initial Particle Concentration $P_0$ | Duration of experiment, $t$ | Average Water Temperature, $T_w$ | Kinematic Viscosity, $\nu$ | Length of Roughness Elements, $l_R$ | Number of Roughness Elements, $N_R$ | Reynolds Number, $Re_c$ | Particle Ratio, $R$ |
|---|---|---|---|---|---|---|---|---|---|---|---|---|---|---|---|
| | | | [m] | [m] | [m $s^{-1}$] | [m] | [$s^{-1}$] | [# $m^{-3}$] | [s] | [C] | [$m^2$ $s^{-1}$] | [mm] | [#] | -- | -- |
| 10-Oct-02 | 10 | 5 | 0.0127 | 1.94E-04 | 0.018 | 0.095 | 0.0026 | 5.4E+07 | 480 | 20 | 9.82E-07 | 1.5 - 2.0 | 60 | 233 | 0.015 |
| 7-Nov-02 | 11 | 3 | 0.0127 | 1.94E-04 | 0.018 | 0.095 | 0.0026 | 5.4E+07 | 480 | 21 | 9.58E-07 | 1.5 - 2.0 | 144 | 239 | 0.015 |
| 14-Nov-02 | 12 | 5 | 0.0127 | 1.94E-04 | 0.010 | 0.09 | 0.0025 | 5.7E+07 | 480 | 20 | 9.75E-07 | 1.5 - 2.0 | 60 | 130 | 0.015 |

# Chapter 3

# Results and Discussion

This chapter will be submitted to *Limnology and Oceanography* as
"Observations of particle capture on a cylindrical collector: implications for particle accumulation and removal in aquatic Systems"
under the following authorship:
Molly R. Palmer, Heidi M. Nepf, Thomas J.R. Pettersson, and Josef D. Ackerman

### 3.1 Introduction

The capture of suspended particles by submerged structures is important to biological cycles and chemical fate (Raudkivi 1998; Patterson and Black 1999; Elliott 2000). Biologically, transport of suspended particles is important in the life cycles of many species. Settlement of planktonic larvae is dictated, at least in part, by the physics of particle motion and substrate encounter (e.g. Butman 1987). For example, Eckman (1983) showed that benthic recruitment is strongly dependent on the presence and numerical density of stem structures. Harvey et al. (1995) provided experimental support for hydrodynamic controls of bivalve larvae settlement onto filamentous branches of benthic algae. In addition, submarine pollination relies on the encounter rate of pollen with individual vegetative elements. Indeed, Ackerman (1995) suggested pollen shape evolved in response to the physics of transport associated with flow around specific plant morphologies.

Chemical fate is often determined by the fate of suspended particles because pollutants such as heavy metals tend to adsorb to suspended particles (Vaithiyanathan et al. 1993; Sansalone and Buchberger 1997). It has long been held that vegetated zones promote particle removal by enhancing residence time (Knight and Kadlec 1999) and reducing resuspension (Lopez and Garcia 1998). Indeed, Gacia et al. (1999) observed that retention of particles by a seagrass meadow is up to 15 times greater

than barren bed. Moreover, some observational studies suggest that capture of particles onto vegetative surfaces is an additional potential mechanism for removing particles (Reay 1972; Stumpf 1983; Jordan et al. 1986; Leonard 1995). For example, Leonard et al. (1995) observed that the capture of sediment on the stems and leaves of *Juncus roemerianus* contributed up to 10% of the total sediment deposition to a tidal marsh. Stumpf (1983) observed that 80% of the suspended material carried by flood waters disappeared within 12 m of the tidal creek, and showed that sediment found on the stems of *Spartina alterniflora* accounted for 50% of this loss. Finally, Hosokawa and Horie (1992) observed that for the same depth and flow speed the addition of artificial reeds increased particle removal by 38%. These examples suggest that physical filtration by plant structures plays some role in particle removal in aquatic systems. Indeed, the capture of particulates by terrestrial plants is already recognized for its impact on air quality (Beckett 1998).

To examine particle capture by submerged elements we begin with a simple cylindrical collector. A cylindrical geometry approximates a variety of natural collectors such as: reed-like wetland vegetation (e.g. *Spartina alterniflora*, *Phragmites australis*); submerged benthic plants and algae (Harvey et al. 1995); and cilia, bristles, tube-feet and other filamentous structures of suspension feeders (Shimeta and Jumars 1991; Wildish and Kristmanson 1997; Riisgard and Larsen 2001). The relevant length scale for flow around a cylinder is the diameter, $d_c$, and flow structure is defined by the collector Reynolds number, $Re_c = ud_c/v$, where $u$ is flow velocity and $v$ is kinematic viscosity. In aquatic systems, $Re_c$ typically ranges from 1 to 1000. Collector diameters can range in size from 1 mm (algal epibenthic collector; see e.g. Harvey et al.1995) to 2 cm (diameter of a large wetland plant stem; e.g. Hotchkiss 1972). Flow velocity $u$ ranges from 0.1 cm $s^{-1}$ to 10 cm $s^{-1}$, and particle sizes reported in the literature range from $d_p$ = 20 to 2000 $\mu$m (Shimeta and Jumars 1991). We use these parameters to examine particle capture on smooth and rough cylindrical collectors in a laboratory flume to better understand particle capture in aquatic systems.

### 3.2 Particle Capture in Aquatic Systems

A wealth of literature exists to explain particle capture by a single cylinder at the two limits of creeping and potential flow, defined by $Re_c$ <1 and $Re_c$ >1000, respectively. For a more complete review, please see Rubenstein and Koehl (1977), Spielman (1977), Shimeta and Jumars (1991), and Pettersson et al.(In Prep). However no analytical solutions exist for the intermediate range of $Re_c$=1-1000, which is of most interest in aquatic systems.

The capture of particles onto a collector is typically described by the efficiency, $\eta$. For a collector of diameter $d_c$, $\eta$ is defined as $b/d_c$, where $b$ is the upstream span of particles that are ultimately captured on the collector. As shown in Figure 3-1, $\eta$ represents the fraction of particles removed from the volume of water passing through the projected area of the cylinder. From previous work at the potential and creeping flow limits, efficiency is understood to be a function of $Re_c$, particle specific gravity, $s$, the particle ratio $R$ (ratio of particle diameter, $d_p$, to collector diameter, $d_c$) and the Stokes number, $Stk$. Stokes number is an inertial parameter defined as the ratio of stopping distance, $l_s$, to cylinder radius. Stopping distance is the additional distance a particle would travel under its own inertia if the fluid were instantly brought to rest. Specifically, $l_s$ is a function of particle density, water density and water viscosity. However, the Stokes number is not an additional independent parameter as it can also be expressed in terms of $Re_c$, $R$, and $s$:

$$Stk = \frac{1}{9} Re_c R^2 (s-1). \tag{3.1}$$

Generally, prediction of $\eta$ considers only how a particle encounters a collector. In this paper, we assume that all encounters will lead to particle capture, such that encounter efficiency and capture efficiency are the same. This is a reasonable first-order assumption for aquatic plants and submerged collectors, because the sticky periphyton layer (consisting of epiphytes and organic biofilm) that grows on submerged surfaces facilitates particle retention (e.g., Borowitzka and Lethbridge 1989; Guarraci 1999). In our experiments we use a coating of grease on the cylinder to guarantee this condition is met.

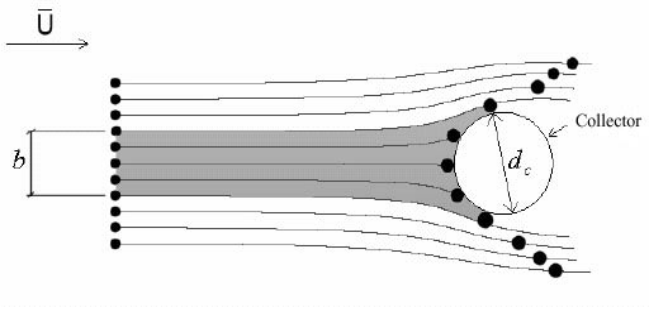


Figure 3-1. Definition of capture efficiency. Capture efficiency $\eta=b/d_c$, where $b$ is the width of particles in the flow upstream of the cylinder that will be captured, and $d_c$ is cylinder diameter. $b$ is evaluated at an upstream point at which the flow doesn't yet appreciate any effects from the cylinder.

Particle capture may occur by four primary mechanisms: direct interception, inertial impaction, gravitational deposition, and diffusional deposition (Rubenstein and Koehl 1977; Spielman 1977). Direct interception, $\eta_R$, describes capture due to streamline kinematics. If a particle traveling on a streamline approaches a collector within one particle radius, the particle will make contact with the collector and be captured. Equations have been developed to describe this capture at creeping flow ($Re_c$<1) and potential flow ($Re_c$>1000). For creeping flow capture efficiency due to direct interception to a smooth cylinder is:

$$\eta_R = \frac{1}{(2 - \ln Re_c)}\left[(1+R)\ln(1+R) - \frac{R(2+R)}{2(1+R)}\right] \approx \frac{R^2}{(2 - \ln Re_c)} \qquad \text{creeping flow (3.2)}$$

as developed by Langmuir (1942) and Fuchs (1964) based on work by Lamb (1932). The rightmost portion of the equation is valid for $R$<0.01. Fuchs (1964) also derived an expression for direct interception to a smooth cylinder based on potential flow:

$$\eta_R = 1 + R - \frac{1}{(1+R)} \approx 2R \qquad \text{potential flow (3.3)}$$

where, again, the simplification on the right side of the equation is valid for $R$<0.01.

Inertial impaction occurs when a particle's inertia causes it to deviate from a streamline and collide with the collector. Aerosol theory asserts that there is a critical Stokes number, $Stk_{crit}$, below which inertial impaction is negligible. For potential flow past a cylinder $Stk_{crit} = 0.125$ (Langmuir and Blodgett 1946; Fuchs 1964). Gravitational deposition occurs when particles settle out of the water column onto horizontal surfaces. Diffusional deposition arises from any random process (i.e. Brownian motion, turbulence) that leads particles to deposit on a collector. Natanson (1957) developed the following equation for diffusional deposition efficiency, $\eta_D$, for creeping flow:

$$\eta_{\mathrm{D}} = \frac{1.17\pi D^{2/3}}{u d_c}\left[\frac{Re_c \nu}{2(2-\ln Re_c)}\right]^{1/3} . \qquad \text{creeping flow} \quad (3.4)$$

Particle diffusion, $D$, is described by:

$$D = (\kappa T)/(3\pi\mu d_p) \qquad (3.5)$$

where $\kappa$ is the Boltzmann constant, $T$ is absolute temperature, and $\mu$ is fluid viscosity (Elimelech et al. 1995).

The capture efficiency defines the rate at which particles collect on a surface, which is of interest in pollination and suspension feeding, as well as the rate at which particles are removed from the water column, which is of interest in chemical fate. Consider a cylinder of length $l_c$. Let $P$ be the number concentration (# $m^{-3}$) of particles in the water. Then the flux, $F$, of particles approaching the cylinder within the region defined by the cylinder's frontal area is:

$$F = P u d_c l_c \qquad (3.6)$$

The number concentration $P$ is equal to mass concentration, $C$, divided by mass of one particle (volume of one particle, $V_p$, times density of particles, $\rho_p$):

$$P = \frac{C}{V_p \rho_p} . \qquad (3.7)$$

Recall that we define $\eta$ as the fraction of particles approaching within the frontal area defined by (3.4) that are ultimately captured. Then the rate at which particles are captured on the cylinder (and removed from the water column) is:

$$\frac{dN_c}{dt} = \eta P u d_c l_c . \tag{3.8}$$

where $N_c$ is the number of particles captured on the collector over a given duration, $t$.

Finally, previous capture theories have only considered smooth collectors, e.g. (3.2) and (3.3) given here. However, aquatic vegetation often grows an epiphytic layer on its submerged surfaces, creating uneven surfaces that may range from micrometers to many millimeters in scale (Borowitzka and Lethbridge 1989; Wetzel 2001). In addition, many suspension feeders have roughness or protuberances on their collectors (see review in Wildish and Kristmanson 1997). Roughness elements on a collector surface can affect capture directly, by providing additional surface area, or indirectly, by altering the local flow field. Here, we conduct a preliminary assessment of the impact of roughness on capture efficiency by considering both smooth and rough cylinders.

### 3.3 Experimental Methods

In this study we use laboratory experiments to observe the capture of particles by rough and smooth cylindrical surfaces over the range $Re_c$ = 50 – 500. The total capture efficiency will depend only on $Re_c$ and $R$ because, for a number of reasons, direct interception is the only relevant capture process. Firstly, Stokes numbers range from $Stk = 3 \times 10^{-5}$ to $4 \times 10^{-4}$, which is significantly smaller than $Stk_{crit}$, so that the contribution to capture by inertial impaction is negligible and we do not consider any dependency on specific gravity, $s$. In addition, the vertical orientation of the collector precluded gravitational deposition. While there is no analytical expression for diffusional deposition at $Re_c$ =50-500, we can estimate $\eta_D$ for creeping flow from (3.4). Since $\eta_D$ is inversely proportional to $u$, this estimate is an upper bound for $\eta_D$ in our experiments. From (3.4) and (3.5), we find that at $Re_c$ = 0.1, diffusional deposition efficiency for the particle and collector sizes we use is on the order of 0.001%. This is an order of magnitude smaller than the capture efficiency we observe, order 0.01% or greater, so we expect that particle capture due to diffusion is negligible in our experiments.

Capture efficiency is measured by allowing particles to collect on a cylinder for duration $t$. By counting the number of particles collected, $N_c$, we estimate $dN_c/dt$ and then infer $\eta$ from (3.8). With $s$=1.03, $P$ decreased significantly over the duration of the experiments due to settling of particles onto the channel bed. We estimate $P(t)$ by the follwoing expression for the flux of particles to the bed:

$$\frac{\partial P}{\partial t} = \frac{-w_s}{h} P \tag{3.9}$$

where $w_s$ is the settling velocity of the particles (or Stokes' velocity) and $h$ is height of water in the flume. Note that removal due to particle capture provided an insignificant reduction in particle concentration (a typical cylinder collected about 50-200 particles per experiment, much less than the millions of particles present in the flume). The decay given in (3.9) assumes that turbulence in the water and mixing produced by the pumps keeps the concentration in the water column uniform over depth. This assumption is later confirmed by continuous measurements of concentration, which decay exponentially as implied by (3.9). The quantity $w_s/h$ is replaced by the constant $k$, henceforth referred to as the settling rate constant, and (3.9) is integrated to derive an expression for concentration decay with time, $t$:

$$P(t) = P_0 e^{-kt} \tag{3.10}$$

Incorporating (3.10) into (3.8) and integrating, we have the expression used to estimate capture efficiency accounting for settling loss:

$$\eta = \frac{N_c k}{P_0 u d_c l_c (1 - e^{-kt})}. \tag{3.11}$$

This assumes capture begins at $t$=0 and ends at time $t$. $P_0$ is the number concentration of particles when the cylinder is inserted.

Experiments were conducted in a flume 2.75 m long, 22 cm wide, and 20 cm high. Water depth, $h$, ranged from 9.0 to 10.5 cm varying with the Reynolds number desired for each experiment. A recirculating flow was generated using up to three different pumps, which included a small centrifugal pump (Micropump, model 101-000), and two peristaltic pumps (Manostat Varistaltic Power Pump model 72-370-000). At the inlet, water was pumped via tubing into a stilling basin and then passed through four

aluminum screens (hole diameter 6.35 mm, 57% open area) to straighten the flow, as is shown in Figure 3-2A.

Velocity profiles were measured with an acoustic Doppler velocimeter (ADV, SonTek 10 MHz) and visualized with dye at multiple longitudinal positions. Based on these profiles and the criteria given below, the longitudinal location 2 m downstream of the inlet was chosen for the cylinder test position. We examined the flow in the lateral and vertical directions to determine the size of the boundary layers and of the central region of uniform flow. At $x$ = 2 m the lateral profile was not fully developed, with the boundary layers extending less than 4 cm from the two side walls. The middle 14 cm of the flow was laterally uniform. Vertically, the bottom boundary layer extended less than 4 cm. Above this, the velocity exhibited no more than 10% variation. Thus we defined a test section of uniform flow between $z$ = 4 cm and the surface. The collector area (see Figure 3-2B) was fully inside this region. The Reynolds number calculated for each trial was based on the average flow velocity from $z$ = 4 to $z = h$. Additionally, velocity profiles and dye visualizations indicated that at a longitudinal position of $x$ = 2m, the suction condition at the outlet did not affect the flow in either the lateral or vertical directions.

An industrial plastic resin (Eliokem Pliolite VTAC-L, $s$=1.03) was chosen for the experimental particles, for its relatively low density, its white color, and the round shape of its particles. The resin was sieved on a shaker table using US standard sieves #70 and #80, having opening diameters of 210 μm and 177 μm, respectively. The fraction captured between these two sieves was used for the experiments; thus the average particle size was estimated as 194 μm ± 17 μm.

12.0 g of sieved Pliolite, measured on a scale (Ohaus model TS400s, readability 0.01 g), was put into suspension using a small amount of surfactant. The suspension was then poured into the flume, which was stirred until the particles spread out over the length of the flume. Since the water recirculated, the same mass of particles could be reused for multiple trials.

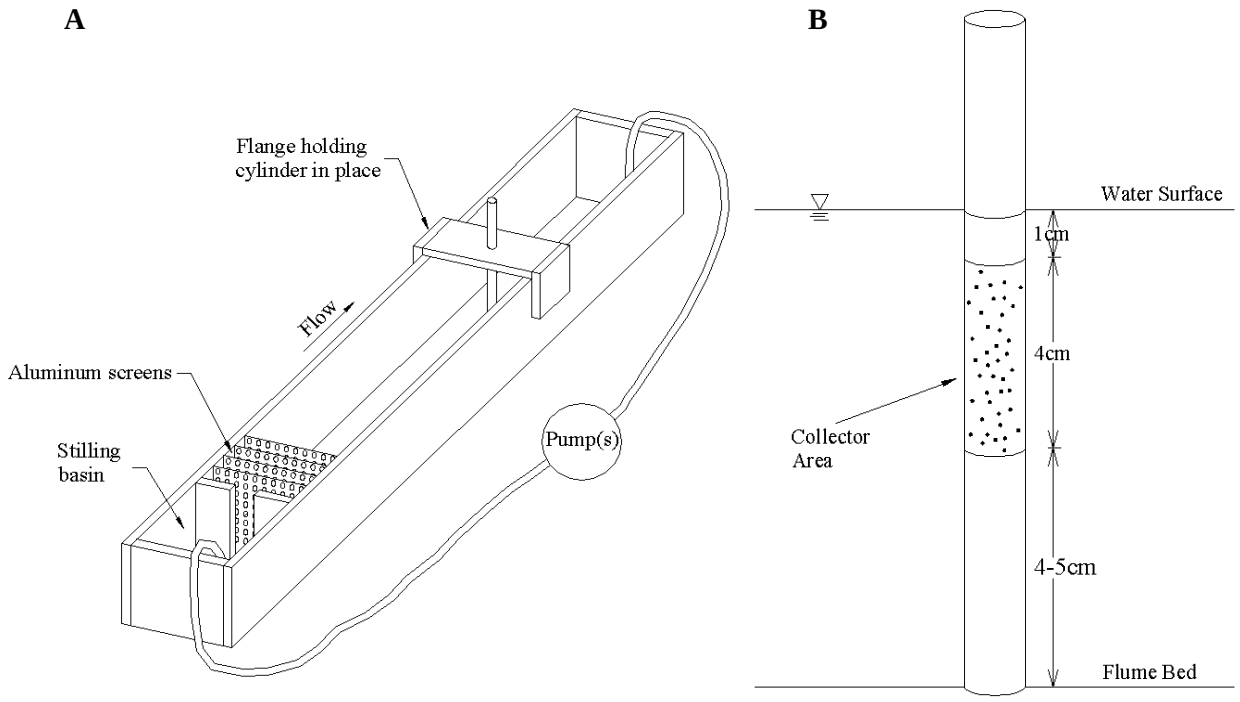


Figure 3-2. Flume setup and cylinder dimensions. (A) In the recirculating flume, water is pumped into a stilling basin and then through a set of four aluminum screens that straighten the flow. The cylinder is held in place from above by a flange at a distance of 2 meters from the inlet. (B) The collector area on the cylinder is a 4 cm-long section located 1 cm below the surface of the water.

*Calculation of settling rate* – We employed the SonTek ADV to monitor the declining concentration of particles in the flume. An ADV measures flow velocity by observing the Doppler shift in acoustic waves reflected off particles traveling with the flow. The probe sends out an acoustic pulse at a known frequency and records the change in frequency as the pulse is returned. The strength of the returned signal, measured in dB, is a function of concentration of particles in the flow. Furthermore, if size and type of particle are uniform, signal strength is directly proportional to the concentration (SonTek 1997). Since decibels are on a logarithmic scale, a difference in signal level is converted to a linear ratio of concentrations by:

$$S - S_0 = 10\log\left(\frac{P}{P_0}\right), \tag{3.12}$$

where $S$ is the scattering strength in dB, $S_0$ is the initial scattering strength in dB, and ($P/P_0$) is the ratio of the concentration to initial concentration. The factor of 10 in (3.12) arises because 1 Bel = 10dB. Combining with (3.10), we get the relation:

$$S - S_0 = 10\log\left(e^{-kt}\right), \tag{3.13}$$

which reduces to a linear equation having the form:

$$S = [S_0] - [10k\log(e)]t. \tag{3.14}$$

This linear equation is fitted to observed scattering strength measurements to estimate the settling rate, $k$.

Scattering strength and particle capture efficiency were not measured simultaneously because the presence of the ADV probe tip in the water was disruptive to the flow. Instead, two replicate concentration records were measured prior to each set of capture experiments. Procedures for taking a concentration record and performing a particle capture trial were identical, the only difference being the presence of the ADV probe tip or the collector cylinder. Because of this, we were confident that the concentration measurements taken prior to each experiment set were indicative of the settling rates in the particle capture trials. To ensure that all particles settled out of the flume, each ADV record lasted 40 minutes, which is more than four times the average experiment duration. The sampling rate of each record was 10 Hz. A typical record of scattering strength vs. time is shown in Figure 3-3.

For each scattering strength record, a linear regression based on 12,000 points gave an $r$-squared correlation of greater than 0.57. Standard errors associated with calculating the intercept and slope of the line were always <1%, so uncertainty in calculating $k$ was very low. Based on (3.14), the slope $m$ of the linear regression yields the settling rate $k=m/(10\log(e))$.

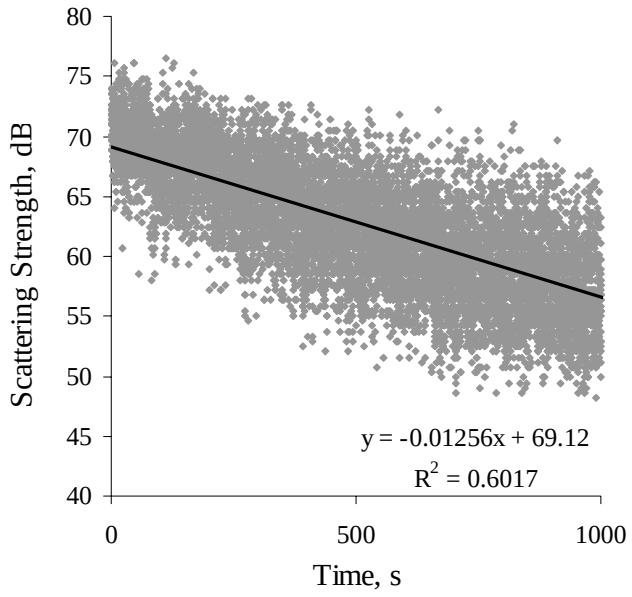


Figure 3-3. Sample ADV record of scattering strength over the duration of an experiment. ADV samples points ( ◆ ) were taken at a rate of 10 $s^{-1}$. A linear fit (solid line) to this equation of the form $S=S_0-mt$ yields an initial signal level of 69.12 ± 0.06 dB and a settling rate $k = m/[10\log(e)]$ = (2.89 ± 0.02) × $10^{-3}$ $s^{-1}$.

*Smooth Experiments* – Three different size Delrin® cylinders of diameters 0.635 cm, 1.27 cm, and 2.54 cm were used as smooth collectors. The manufacturer's tolerance on the Delrin rods is 0.005 cm, and any variation in size of the cylinders was negligible. Three different flow rates were used, yielding a total of nine different collector Reynolds numbers, ranging from 50 to 500, and three different *R* ratios (0.008, 0.016, and 0.03).

Cylinders were prepared by marking off a four-centimeter-long test section. In this section the black Delrin® was left exposed so that the white Pliolite particles would be clearly visible. The rest of the cylinder was covered in white tape. The front of the cylinder, which points directly upstream, was marked with a vertical red line, indicating the zero-degree mark. The cylinder was greased by applying a liberal coating, about 2-3 mm thick, of clear silicone grease (Chemplex silicone compound 710 by NFO Technologies). The excess grease was then wiped off with a paper towel in one pass, leaving a thin, uniform coating of negligible thickness (<<1 mm). An end-on visualization confirms that the thickness is

uniform around the cylinder and is not thick enough to significantly change the diameter of the cylinder. This process was quite repeatable such that the grease layer thickness was constant from trial to trial.

The flume was stirred by hand for about one minute to bring it to fully-mixed conditions. Because flow was very turbulent from the mixing, it was allowed to straighten out for 60 s before the cylinder was lowered into the flume. When inserted in the water, the 4-cm test section began one centimeter below the surface of the water so that surface effects were minimized (see cylinder orientation in Figure 3-2B). The red line at the zero-degree mark was aligned with the upstream, and particles were allowed to collect for a duration ranging from 6 to 10 minutes, depending on how much time was needed for a significant number of particles to collect.

The cylinder was removed at the end of the experiment and allowed to dry. It was then photographed with a 4.1-megapixel digital camera (Sony DSC-S85 Cyber-shot®). Although Pliolite particles are visible to the naked eye and could be counted by hand, taking a digital photo allowed us to magnify the view of the cylinder while collecting photos for future reference. For the smooth experiments, one photo taken from the front was sufficient to photograph almost all the captured particles because capture was limited to ± 50 degrees from the front. During some of the higher Reynolds number experiments, a small number of particles deposited on the back side of the cylinder. These were simply counted by hand, as there were usually fewer than 10.

*Rough Experiments* – The procedure for the rough experiments was the same as for the smooth, except roughness elements were added during the greasing process. Instead of roughening the surface of the cylinder and then greasing it, we found a more uniform and consistent roughness was produced using the grease itself to create roughness elements. These elements retained their shape when inserted into flowing water. A flat nail head was used to apply a dot of grease to the cylinder. The nail head was then pulled away from the cylinder, bringing the grease out to a point and forming a nearly conically shaped roughness element, shown in Figure 3-4A. The diameter at the base of these roughness elements was about 1.5 mm, and the elements protruded a distance of 1.5-2 mm. This scale of roughness was chosen

because it was significantly larger than the particle size and also larger than the estimated boundary layer thickness. Based on numerical calculations (reported in Pettersson et al. In Prep), for the range of $Re_c$ used in the rough experiments, the boundary layer thickness, $\delta$, varied from 0.6 mm to 1.5 mm, depending on the radial position around the cylinder and the Reynolds number.

The roughness elements were placed on the cylinder in two array patterns. Initially, two sets of experiments were conducted using a low-density configuration: this consisted of 8 staggered rows (a row every 45 degrees) around the cylinder, with a total of 60 elements and a density of about 4 elements per $cm^2$, as shown in Figure 3-4B. One experiment set was also conducted at a higher-density roughness pattern of 8 elements per $cm^2$. This pattern was made up of 12 rows (a row every 15 degrees) in an unstaggered pattern, as shown in Figure 3-4C.

With roughness, particle deposition was more spread out than with smooth cylinders, so photographs were taken covering the full 360 degrees of the rough cylinders. During counting a distinction was made between particles that deposited on a roughness element and those that deposited on a smooth area of the cylinder, and detailed information on the spatial distribution of particles was collected.

### 3.4 Results

Table 3-1 summarizes the capture efficiency measured in 12 experiment sets. Each set included five replicate trials. Uncertainty was estimated in two ways: 1) propagated uncertainty was calculated for an individual trial (Taylor 1997); and 2) standard error was computed for the five replicate trials. In Table 3-1, however, only the propagated uncertainty is reported, as it was higher than the standard experimental error for each experiment set.

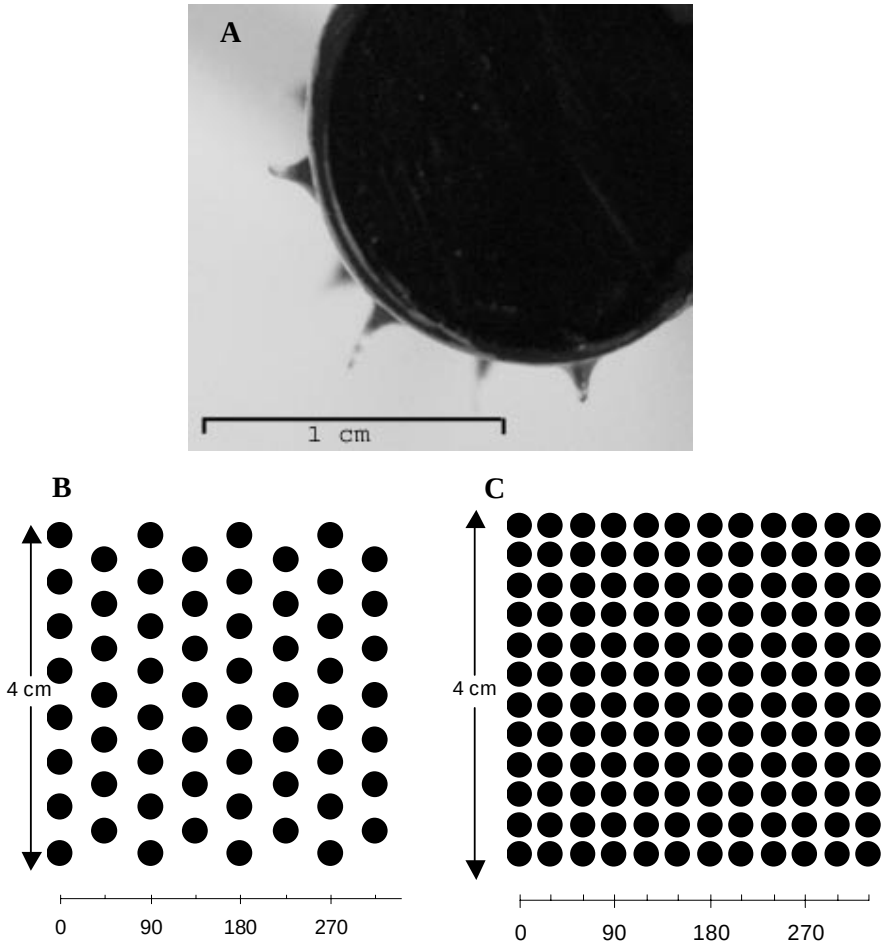


Figure 3-4. Geometry and placement of roughness elements. (A) Cross-sectional view of roughness elements. Applying a small dot of grease to the cylinder and pulling the nail head outward created the conically-shaped elements. The resulting element shape has a base diameter of about 1.5 mm and a protruding length of 1.5 – 2 mm. (B) 'Unrolled' arrangement of roughness elements on the collector area in low-density configuration (4 $cm^{-2}$). The rows are staggered for a total of 60 elements per cylinder. (C) Similar 'unrolled' arrangement for high-density configuration (8 $cm^{-2}$). Here, the rows are not staggered.

Table 3-1. Summary of experiment parameters and results. Twelve sets of experiments were conducted with each having five replicate trials. Collector diameter, $d_c$, is in cm; $Re_c$ is the collector Reynolds number ($Re_c=ud_c/\nu$); and $R$ is the ratio of particle diameter to cylinder diameter ($R=d_p/d_c$). The error reported is based on the propagated uncertainty for one trial.

| | | | | | Capture efficiency, η |
|---|---|---|---|---|---|
| Experiment Set | Type | $d_c$ (cm) | $Re_c$ | $R$ | Mean (%) |
| 1 | smooth | 0.635 | 68 | 0.031 | 0.35 ± 0.05 |
| 2 | smooth | 1.27 | 137 | 0.015 | 0.14 ± 0.02 |
| 3 | smooth | 2.54 | 279 | 0.008 | 0.050 ± 0.008 |
| 4 | smooth | 0.635 | 38 | 0.031 | 0.21 ± 0.03 |
| 5 | smooth | 1.27 | 76 | 0.015 | 0.094 ± 0.014 |
| 6 | smooth | 2.54 | 149 | 0.008 | 0.032 ± 0.005 |
| 7 | smooth | 0.635 | 115 | 0.031 | 0.48 ± 0.07 |
| 8 | smooth | 1.27 | 239 | 0.015 | 0.19 ± 0.03 |
| 9 | smooth | 2.54 | 486 | 0.008 | 0.077 ± 0.011 |
| 10 | rough | 1.27 | 233 | 0.015 | 0.27 ± 0.04 |
| 11 | rough | 1.27 | 239 | 0.015 | 0.42 ± 0.06 |
| 12 | rough | 1.27 | 130 | 0.015 | 0.26 ± 0.04 |

Particle capture efficiencies for smooth cylinders increase with increasing Reynolds number, $Re_c$, and with increasing particle ratio, $R$, as shown in Figure 3-5. However, dependence of $\eta$ on $R$ is stronger than dependence on $Re_c$. For example, $R$ must increase by a factor of 1.5 in order to roughly double capture, but $Re_c$ must increase by a factor of 3 to double capture.

Rough experiment sets 10 and 11 were conducted at the same $R$ and $Re_c$ as smooth experiment set 8. At $Re_c$ =240 and $R$=0.015, the presence of low-density roughness (4 $cm^{-2}$) caused the capture efficiency to increase by 40% (from 0.19% to 0.27%). Using the same parameters with a higher-density roughness pattern (8 $cm^{-2}$) caused capture efficiency to increase by 120% (to 0.42%) in experiment set 11. Experiment set 12 was conducted at $Re_c$=130 (comparable to smooth experiment set 2) to confirm the increasing trend of $\eta$ at a lower $Re_c$. Again, the particle capture efficiency increased by 85% (from 0.14% to 0.26%) with the addition of roughness.

The spatial distribution of particles also differed between smooth and rough cases. For smooth cylinders, more than 95% of the particles captured deposited on the front 100 degrees of the cylinder. At $Re_c$ <200 no particles were observed to deposit on the back side of the cylinder. At $Re_c$ >200, though,

some particles did deposit on the back, but this was less than 5% of the overall number of particles captured. This capture is believed to be a consequence of the vortex generation and shedding that occurs behind a cylinder at higher Reynolds numbers. Particles on the rough cylinders were more spread out, with significant capture to the roughness elements on the sides of the cylinder extending the zone of capture to over 180 degrees of the cylinder's circumference. Similar to the smooth experiments, some capture (less than 5%) was observed on the back of the cylinder, again presumably due to cylinder wake structures. Table 3-2 compares smooth capture, $\eta_{smooth}$ to rough capture, $\eta_{rough}$, and also shows the partitioning of $\eta_{rough}$ into deposition to smooth surfaces ($\eta_{rough,SS}$) and deposition to roughness elements ($\eta_{rough,RS}$). Additionally, capture to the front 100 degrees of the rough cylinder, $\eta_{rough,100}$, is shown, to enable comparison of capture to the front faces of both smooth and rough cylinders.

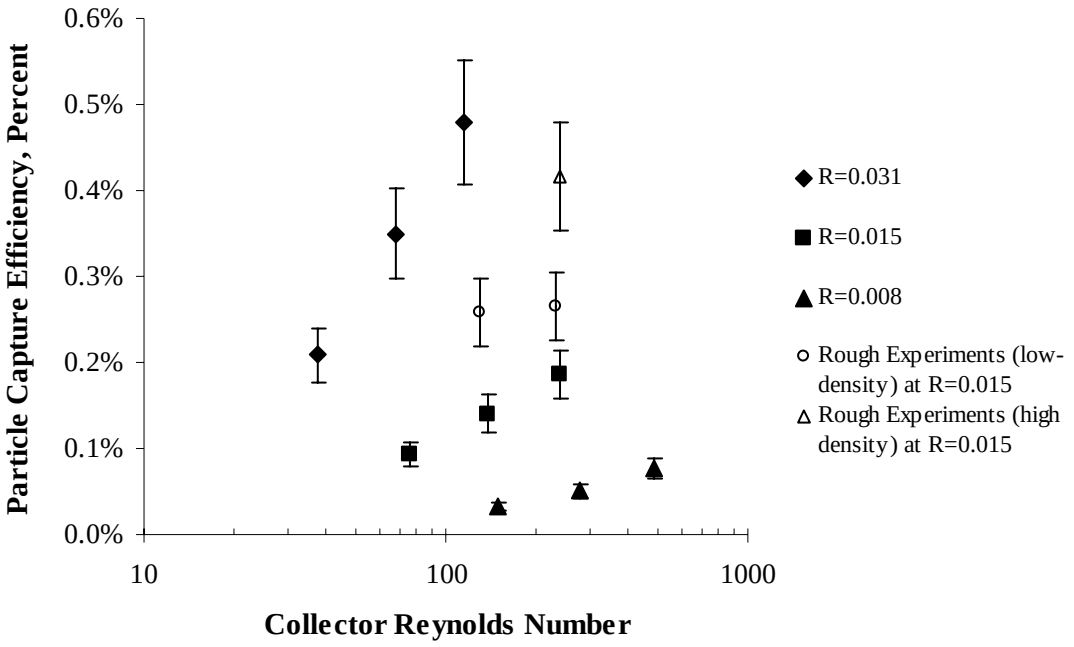


Figure 3-5. Plot of results. The trends for smooth capture are visible in this plot: capture efficiency increases with increasing $Re_c$ and $R$. However, $\eta$ depends much more strongly on R. The three data points for rough experiments all clearly show that for these roughness configurations, $\eta$ is higher than in the analogous smooth case.

Table 3-2. Comparison of smooth and rough capture efficiencies. Capture efficiency from the smooth experiments, $\eta_{smooth}$, is shown, along with four capture efficiencies computed for the corresponding rough experiments. The total amount of capture to the rough cylinder is $\eta_{rough}$; capture only to the smooth surfaces of the rough cylinder is $\eta_{rough,SS}$; capture only to the roughness elements of the rough cylinder is $\eta_{rough,RS}$, and capture to the front 100 degrees of the rough cylinder is $\eta_{rough,100}$. All efficiencies are in percent (%, mean ± standard error).

| Type of Capture Efficiency | $Re_c$=230 | $Re_c$=130 |
|---|---|---|
| $\eta_{smooth}$ | 0.19 ± 0.03 | 0.14 ± 0.02 |
| $\eta_{rough}$ | 0.27 ± 0.04 | 0.26 ± 0.04 |
| $\eta_{rough,SS}$ | 0.13 ± 0.02 | 0.07 ± 0.01 |
| $\eta_{rough,RS}$ | 0.13 ± 0.02 | 0.19 ± 0.03 |
| $\eta_{rough,100}$ | 0.18 ± 0.03 | 0.16 ± 0.02 |

### 3.5 Discussion

*Smooth Surfaces* – In Figure 3-6 the observed capture efficiencies are compared to the theoretical predictions based on creeping flow (heavy dashed lines) and potential flow (thin dashed lines). As anticipated, neither theory is appropriate in the range of $Re_c$=50-500 considered here and representative of conditions in most aquatic systems. However, the observed capture efficiencies fall smoothly between theories suggesting that capture increases monotonically with $Re_c$.

Our measured efficiencies compare favorably to those predicted numerically by Pettersson et al. (In Prep), shown as solid curves in Figure 3-6, although the modeled efficiencies underpredict the observed efficiencies for lower $R$ values. We believe the cause of this underprediction lies with the model's computation of the boundary layer on the cylinder surface. Because the boundary layer deflects streamlines away from the surface, if the scale of the boundary layer, $\delta$, is overpredicted, the number of particles encountering the cylinder will be reduced. Overprediction of $\delta$ will have the greatest effect on the smallest particle ratio ($R$=0.008), consistent with the trend shown in Figure 6.

In any particular aquatic environment the same flow speed and the same mix of suspended particles are available to all potential collectors. Thus, it is useful to consider how capture efficiency varies across collector size, $d_c$, given a fixed value of $u$ and a fixed set of particle characteristics, or e.g. a

single characteristic $d_p$ and $s$. Our observations can be grouped into three series of constant $u$, as indicated by the lines drawn through our data (Figure 3-6). Moving left to right along each line $d_c$ = 0.635 cm, 1.27 cm, and 2.54 cm, respectively, and thus $R=d_p/d_c$ decreases and $Re_c$ increases moving left to right. Very clearly the smaller diameter collectors capture more particles than the larger diameter collectors.

As discussed earlier, we expect direct interception to be a function of $Re_c$ and $R$. Specifically, we look for an empirical relation of the form, $\eta \sim (Re_c)^m (R)^p$. For our nine distinct flow conditions [$Re_c$ = 50-500 and R = 0.008 to 0.03] we find

$$\eta = 0.224(Re_c)^{0.718}(R)^{2.08} \tag{3.15}$$

fits all experimental data to within 10% (Figure 3-7). Consistent with existing theory, the exponents on $R$ and $Re_c$ fall between the leading order values found at creeping and potential flow. To further test the limits of this empirical relation, we considered the numerically determined efficiencies from Pettersson et al. (In Prep) for conditions dominated by direct interception, i.e. their cases $s$ = 1.05 and $R$ = 0.008 - 0.16. The numerical efficiencies at $Re_c$ = 10, 100, and 1000 all conform to (3.15), as shown in Figure 3-7. For $Re_c \leq 1$ the numerical efficiencies diverge from (3.15) and approach (3.2), as expected. By combining these two data sets, we conclude that (3.15) is valid for $Stk < Stk_{crit}$, i.e. direct interception only, and $Re_c$ = 10-1000.

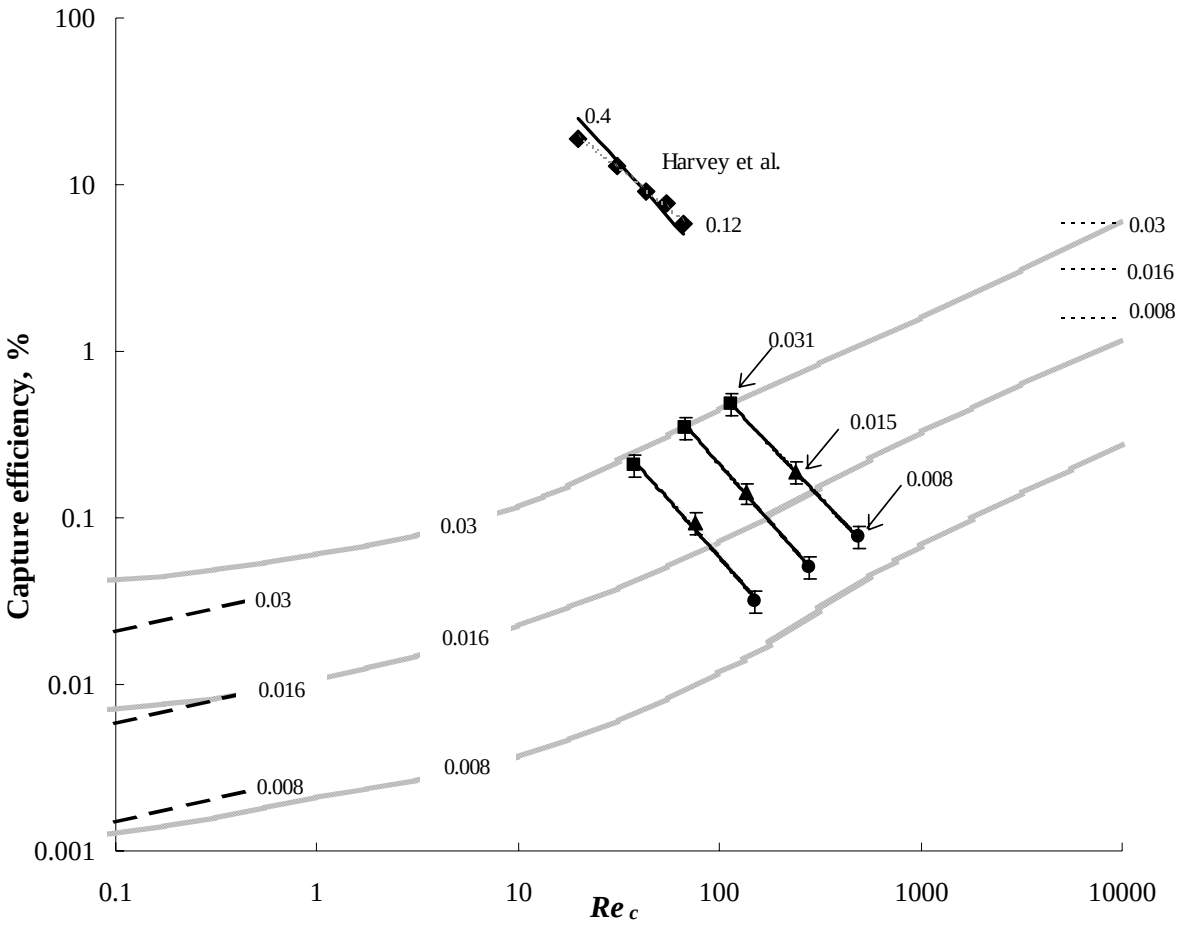


Figure 3-6. Smooth experimental capture efficiency is shown for three *R* ratios: 0.031 ( ■ ); 0.015 (▲); and 0.008 ( ● ). The solid black lines represent power law fits for constant *u* and varying *R*, for which we found a constant exponent of 4/3 for the three fits. The numerical model (Pettersson et al. In Prep) does a good job of predicting the measured trends for capture efficiency (shown by gray lines ( ▬ )*). The creeping flow (thick dashed lines) and potential flow equations (thin dashed lines) cannot be used to predict $\eta$ for $Re_c$=1-1000. Capture efficiencies for a branched structure are taken from Harvey et al. (1995) (◆). Each data point has a different *R*, varying from 0.12 – 0.4. For the observations taken by Harvey et al., the best fit power law ( - - - ) and the fit using an exponent of 4/3 are shown (solid black line), illustrating that the trends observed in our experiments are consistent with those used in the branched experiments. Throughout the figure, points and lines are labeled with corresponding *R*.

*Numerical results are only available for *R*=0.03, 0.016, and 0.008, hence the discrepancy between *R* values in numerical and experimental results.

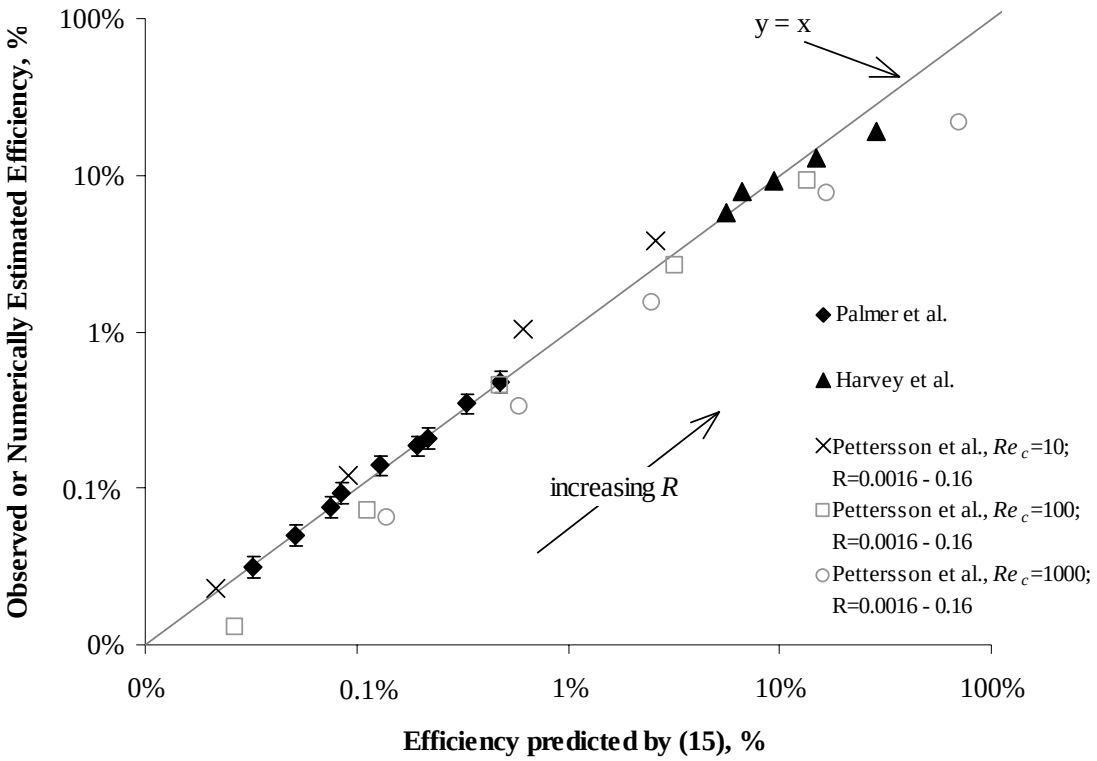


Figure 3-7. Comparison of observed and numerically estimated efficiencies to empirically predicted efficiencies. Observed efficiencies for single-cylinder experiments (black diamonds) are plotted against values predicted by the empirical relationship in (3.15). This empirical relationship also provides good agreement to capture efficiencies on branched structures observed by Harvey et al. (1995) (black triangles) and to numerically estimated efficiencies produced by Pettersson et al. (In Prep) (crosses, open squares, open circles).

The above trends are also seen by Harvey et al. (1995) for branches of different diameter within a single structure. Harvey et al. conducted field and laboratory experiments to study the passive accumulation of larvae on epibenthic structures. The larvae of marine benthic invertebrates settle onto epibenthic structures by active and passive accumulation. Active accumulation occurs when larvae chemically or biologically moderate their path, whereas passive accumulation occurs when only hydrodynamic processes control their transport. Harvey et al. investigated the latter case by performing experiments with artificial particles and branch structures. They created filamentous branch structures, shown in Figure 3-8, starting with a single branch that bifurcated into two, with each successive branch

bifurcating into branches of progressively smaller length and diameter. Each structure had five branch diameters, ranging from 0.5 – 1.7 mm. Their study used one flow speed of 5 cm $s^{-1}$ and 200 μm-diameter particles of specific gravity $s$=1.4. The study reported particles per unit area of branch, mass flow rate of particles, and cylinder geometry. From these parameters one can estimate the capture efficiency for each branch diameter. These results, along with $Re_c$ and $R$ for each branch, are shown in Table 3. Consistent with the single cylinder results reported earlier, the greatest capture efficiency is associated with the smallest branch, and decreases monotonically to the largest branch. In addition, (3.15) correctly predicts the capture to individual branches within the structure, as shown in Figure 3-7. This suggests that (3.15) can be used to predict efficiency for collector geometries more complex than single cylinders and for larger $R$ than we examined in this study.

Finally, we compared the Harvey et al. data set to numerically predicted capture efficiencies for individual cylinders, as reported in Table 2 of Pettersson et al. (In Prep). Capture efficiencies observed for branched elements (Harvey et al. 1995) are consistent with values interpolated and extrapolated from Pettersson et al. (In Prep) as shown in Table 3-3. Based on the agreement of the power law fits and numerical predictions, we believe that although $R$ is higher than in our experiments, capture efficiency in the branched experiments exhibits the same trends as in our single-collector experiments. Importantly, this indicates that our results for single cylinders may be used to successfully predict capture efficiency in systems containing multiple cylinders with complex arrangements.

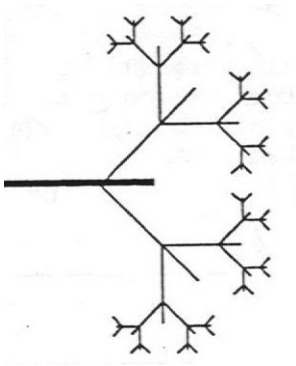

Figure 3-8. Branch structure used by Harvey et al. (1995) in flume experiments simulating larval settlement. Multiples of the above 2D structure were assembled to make a 3D branch structure. Each one has branch diameters ranging from 0.5 – 1.7 mm, with diameter decreasing as amount of branching increases.

Table 3-3. Capture Efficiencies computed from data collected by Harvey et al. (1995). Particle ratio, *R*, is what most influences $\eta$, with the largest *R* ratios (the smallest branches) having the highest capture efficiencies. $\eta_{num}$ is the efficiency predicted by a numerical model created by Pettersson et al.(In Prep).

| $d_c$ (mm) | $Re_c$ | $R$ | $\eta$ (%) | $\eta_{num}$ (%) |
|---|---|---|---|---|
| 0.5 | 20 | 0.40 | 19 | 20 * |
| 0.8 | 31 | 0.25 | 13 | 10 * |
| 1.1 | 43 | 0.18 | 9.1 | 8 * |
| 1.4 | 55 | 0.14 | 7.8 | 6 ** |
| 1.7 | 66 | 0.12 | 5.8 | 5 ** |

* extrapolated from numerical results
** interpolated from numerical results

*Particle removal in a typical wetland* – As previously discussed, particle capture by vegetation has been indicated as one mechanism by which wetlands reduce suspended particle load (Stumpf 1983; Hosokawa and Horie 1992; Leonard et al. 1995). To quantify the potential importance of this mechanism, we consider a model that accounts for capture to stems as well as gravitational settling in a typical emergent *Spartina alterniflora* coastal wetland. The equation for capture to a single collector, (3.8), is rewritten in a per-unit-volume form, where *V* is volume of water:

$$\frac{1}{V}\frac{dN_c}{dt} = \frac{\eta P u d_c l_c}{V} = \eta P u d_c l_c' \tag{3.16}$$

$N_c/V$ is equal to $P$. We define $l_c'$ as the total collector length per unit volume, or $l_c/V$. Additionally, particles are lost from the water column through settling. We employ a settling model identical to (3.9) in which we assume turbulence keeps the concentration vertically uniform, so that loss due to settling is first order. The total rate of change of particle concentration is then:

$$\frac{dP}{dt} = -\eta P u d_c l_c' - \frac{w_s}{h} P \tag{3.17}$$

We let $K_C = \eta u d_c l_c'$ and $K_S = w_s/h$, where $K_C$ and $K_S$ are the rate constants for capture and settling, respectively. Finally, after integration, the solution for concentration in the water column is:

$$\frac{P}{P_0} = \exp\left(-\left(K_c + K_S\right)t\right) \tag{3.18}$$

To examine the importance of particle capture in a wetland, we compare the removal by the combined mechanisms of capture and settling to the removal achieved by settling alone. We define the variable $L_{50}$ as the length of wetland required for the concentration of particles to be reduced by 50%. From (3.18),

$$L_{50} = 0.693\left(\frac{u}{K_C + K_S}\right) \tag{3.19}$$

For settling alone, $K_c$ is set to zero in (3.19).

The physical parameters, shown in Table 3-4, were chosen based on typical values observed in real wetlands (e.g. Valiela et al 1978), with the constraint that $Re_c$ and $R$ be appropriate for use with (3.15). We used two representative particle diameters, 50 μm and 300 μm, as well as three flow velocities of 1, 5, and 10 cm $s^{-1}$. Although larger and smaller values of $d_p$ and $u$ might be observed in wetlands, the chosen values give $R$= 0.006 - 0.6 and $Re_c$= 6-1000, ranges over which (3.15) is shown to be valid. *S. alterniflora* has two forms, called short and tall, the primary difference being that the stem diameter and height are smaller in the short form. We estimated $d_c$ and $l_c'$ using areal stem density, stem

height, and histograms of stem diameter as reported by Valiela et al. (1978). The branches of *S. alterniflora* also contribute to capture. We assume that the branch diameter is one-half the stem diameter, and that submerged branch length is one-third of the submerged stem height. For each bin of stem diameters given in the histogram (Valiela et al 1978), we computed $R$ and $Re_c$ and found $\eta$ from (3.15). We then computed $K_C$ for each bin of diameters. The total rate constant is simply the sum of the values for each bin. We computed $w_s$ using standard equations for terminal velocity of a settling sphere (see e.g. Streeter and Wylie 1985). The height, $h$, of water in the wetland was taken to be 15 cm, and all the vegetation was assumed to be emergent (i.e. stem height > 15 cm). $L_{50}$ was then calculated from (3.19) for particle removal by settling and filtration combined. For comparison, $L_{50}$ contributed by settling alone was calculated from (3.19) with $K_c = 0$.

$L_{50}$ is plotted against the depth-averaged velocity in Figure 3-9. For both particle sizes, removal by particle capture is significant for $u \geq 3$ cm s$^{-1}$. Above this, the rate of removal due to particle capture is an order of magnitude or greater than the rate of removal due to settling. In general the decrease in $L_{50}$ is more significant for the short form, reflecting both the higher stem density and smaller stem diameter (higher $R$) typical of this form. This example indicates that particle capture can contribute significantly to the removal of light particles and pathogens, i.e. with $s = 1.03$, as considered here.

Table 3-4. Parameters for wetland removal model. Wetland vegetation was modeled from stand characteristics of short form and tall form *Spartina alterniflora* reported by Valiela et al. (1978). $d_p$, $d_c$, and $u$ were chosen so that $Re_c$ and $R$ met the requirements of (3.15).

| | Short Form | Tall Form |
|---|---|---|
| $Re_c$ | 6 - 300 | 10 - 1000 |
| $R$ | 0.02 - 0.6 | 0.006 - 0.15 |
| $u$ | 1, 5, 10 cm s$^{-1}$ | 1, 5, 10 cm s$^{-1}$ |
| $d_p$ | 50, 300 μm | 50, 300 μm |
| $d_c$ | 0.5 - 3 mm | 2 - 9 mm |

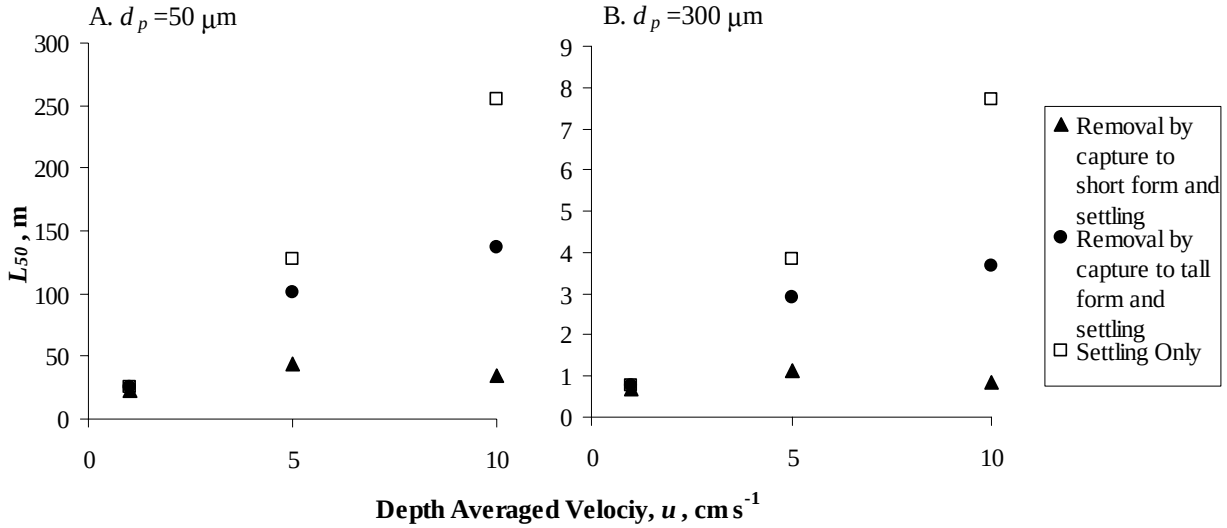


Figure 3-9. Particle removal due to vegetation filtration and settling in a typical wetland. $L_{50}$ is the length of wetland necessary to reduce the initial concentration by 50%, due either to settling alone (the base case) or to the combination of settling and vegetation filtration. Above $u$=3 cm s$^{-1}$, capture to both short and tall form *Spartina alterniflora* becomes a significant mechanism of particle removal.

*Rough Surfaces* – Although this study is not extensive enough to create a complete picture of how particles interact with roughness, some preliminary conclusions can be drawn from our results. For the type and size of roughness used here, particle capture efficiency increases with roughness. However, capture to the front face of the rough cylinder occurs at rates that are nearly identical to the smooth case. Specifically, as shown in Table 3-2, for the same Reynolds number, the capture to the front 100 degrees of the rough cylinder ($\eta_{rough,100}$) is nearly the same as the total capture efficiency for the smooth case ($\eta_{smooth}$). For $Re_c$=230, $\eta_{smooth}/\eta_{rough,100} = 1.0 \pm 0.1$, and for $Re_c$ =130, $\eta_{smooth}/\eta_{rough,100} = 0.87 \pm 0.07$. The increase in capture from smooth to rough, then, is the capture that occurs directly to individual roughness elements that protrude into the flow, especially on the sides of the cylinders. That is, the roughness elements function separately from the main collector and have their own associated capture efficiency. If we take $d_{element}$ to be the average diameter of the conical roughness element, then the

particle ratio of the roughness element, $R_{element}$, is 0.2, which is significantly higher than any $R$ value associated with the main cylindrical collectors. Based on $\eta$'s dependency on $R$, we expect $\eta_{\text{element}}$ to be much higher than $\eta$ we measure for the main cylinder. We estimate $\eta_{\text{element}}$ by using the spatial distribution data shown in Table 2: $\eta_{rough,RS}$ reflects the total number of particles that deposited on roughness elements. We divide that quantity by the total number of roughness elements that captured particles and have an estimate of $N_E$, the number of particles captured by a single roughness element. Then we use (3.8) and estimates of the element geometry to compute $\eta_{\text{element}}$. This analysis was only completed for the low-density roughness configuration because spatial distribution data was not available for the high-density experiments. For $Re_c$=230, $\eta_{\text{element}} = 3 \pm 1\%$, and for $Re_c$=130, $\eta_{\text{element}} = 4 \pm 1\%$. The uncertainty in these estimates derives predominantly from deciding how many of the roughness elements on a cylinder captured particles. These element efficiencies are indeed significantly higher than the capture efficiencies of the main cylinders (the highest capture efficiency observed for a main collector was 0.48%). Additionally, we observed dense clusters of particles on the roughness elements (see e.g. Figure 3-10), supporting our belief that they have a high capture efficiency and that the process of capture to them is independent from capture to the large collector. Therefore we believe that the extra capture created by these high-efficiency roughness elements is what serves to augment overall capture to the rough cylinder.

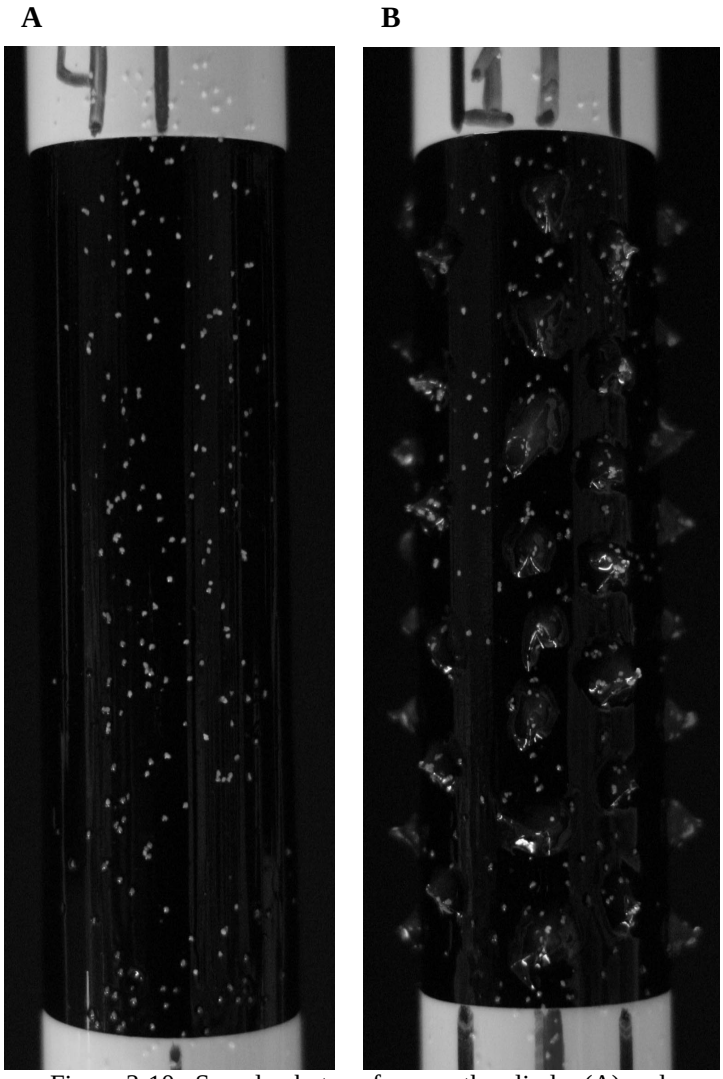


Figure 3-10. Sample photos of a smooth cylinder (A) and a cylinder with roughness elements (B). Except for the added roughness elements, experiment parameters for both were identical ($Re_c$=230, $R$=0.015, $d_c$=1.27 cm). The rough cylinder's capture efficiency is 40% higher than the smooth cylinder's. Capture on the rough cylinder is more spread out over the circumference of the cylinder: particles cover the front 100° of the smooth cylinder, while they cover about 180° of the rough.

We hypothesize, however, that not all arrangements of roughness will lead to an increase in capture efficiency. Adding roughness elements to a smooth cylinder increases the drag of that cylinder, which in turn, changes the flow field. The streamlines will move away from the cylinder boundary as more drag is added.

The drag forces on a smooth and rough cylinder ($D_{smooth}$ and $D_{rough}$, respectively) are:

$$D_{smooth} = \frac{1}{2}\rho C_D d_c l_c U^2 \tag{3.20}$$

$$D_{rough} = \frac{1}{2}\rho C_{D_o} d_c l_c U^2 = \frac{1}{2}\rho C_D d_e l_c U^2 \tag{3.21}$$

where $\rho$ is density of water, $C_D$ is drag coefficient for a smooth cylinder, $C_{Do}$ is drag coefficient for a rough cylinder, $d_e$ is the effective collector diameter (defined below), and $U$ is velocity. $C_D$ is a function of $Re_c$ and $C_{Do}$ is a function of $Re_c$, relative roughness, $\varepsilon/d_c$ (where $\varepsilon$ is a roughness scale), and roughness density, $n$. Far upstream of the cylinder, though, the flow does not see the particular roughness present on the cylinder. The flow simply adjusts its streamlines based on the drag that is produced by the composite structure downstream. For the smooth cylinder, the streamlines deviate in accordance with the drag produced by a cylinder of diameter $d_c$. For a rough cylinder of diameter $d_c$ and roughness length ε, the streamlines deviate farther from the cylinder due to the drag caused by the roughness. The flow perceives the increase in drag as if it were an increase in diameter of the cylinder. We define $d_e$, then, as the effective diameter due to roughness for a cylinder of base size $d_c$. Then we can say that for smooth and rough cylinders, $C_D$ is the drag coefficient of a smooth cylinder of diameter $d_c$ or $d_e$, and is a function of $Re_c$ only. In general, the difference in $d_c$ and $d_e$ will be small, and Reynolds number will not change greatly. To first order, then, $C_D$ in (20) and (21) will be equivalent. Then $D_{smooth} \propto d_c U^2$ and $D_{rough} \propto d_e U^2$ and for the same flow conditions,

$$\frac{d_e}{d_c} = \frac{D_{rough}}{D_{smooth}}. \tag{3.22}$$

If roughness is present (meaning drag is increased), $d_e$ will be greater than $d_c$ and streamlines will be pushed outward. How this influences capture, though, depends on how the increase in diameter compares to the scale of the roughness. If the drag causes the effective diameter to increase by an amount less than $2\varepsilon$ ($\varepsilon$ is the roughness length scale of the elements), then the roughness elements will protrude beyond the effective diameter, allowing particles from passing streamlines to collect on them (see Figure 3-11A):

$$d_c + 2\varepsilon > d_e, \quad \text{capture enhanced} \tag{3.23}$$

The presence of this type of roughness configuration enhances capture compared to the smooth cylinder. Conversely, when the drag from roughness becomes so significant that it pushes the effective diameter beyond the roughness elements, streamlines bypass the roughness layer and capture to the cylinder will not be enhanced:

$$d_c + 2\varepsilon < d_e, \quad \text{capture diminished} \tag{3.24}$$

Capture to the cylinder will proceed as if it is a smooth cylinder of diameter $d_e$, as shown in Figure 3-11B. Although $Re_c$ is higher for the cylinder of diameter $d_e$, the particle ratio $R$ decreases and overall capture will be reduced. When the density of roughness is so high that this scenario occurs, having roughness provides no increase in capture efficiency and could actually be disadvantageous to the collector.

For each of our roughness experiments, capture was decidedly enhanced (Figure 3-5), indicating that the flow was operating in the regime of (3.23). To confirm the model, we estimated the drag created by the elements. Each element was modeled as a cylinder (providing a more conservative estimate) and drag was computed based on standard drag coefficients for a cylinder (see Hoerner 1965). Furthermore, when the aspect ratio of a cylinder is small ($L/d$<2.5, where $L$ is the length of the cylinder and $d$ is diameter), separation and vortex shedding at the end of the cylinder cause the mean drag coefficient to decrease when compared to a cylinder of larger aspect ratio ($L/d$>2.5). For a finite-span cylinder with $L/d$ =1, Sin and So (1987) show this reduction is about 40-50%. Since the roughness elements have an aspect ratio of $L/d$≈1, we apply a 50% correction.

We then computed the drag created by the elements and by the main cylinder to calculate the effective increase in diameter using (3.22). For roughness density 4 cm$^{-2}$, $d_e$=1.37 and for roughness density 8 cm$^{-2}$, $d_e$=1.50 cm. In all cases the roughness elements protruded 1.5 – 2 mm from the cylinder surface meaning $d_c + 2\varepsilon$ = 1.27 cm + (0.3 - 0.4) cm ≈ 1.57 - 1.67 cm. Thus (3.23) is satisfied, and the model predicts capture will be enhanced, consistent with our observations.

We wanted to increase $d_e$ such that $d_c + 2\varepsilon < d_e$, but could not pack the conical roughness elements any tighter than 8 $cm^{-2}$. Even though our experiments do not confirm the trend of reducing capture when sufficient roughness is added, such a trend would be consistent with previous results by Cheer and Koehl (1987), who modeled flow through finite rows of cylinders. They showed that the flow between adjacent cylinders was effectively eliminated when the cylinder Reynolds number was less than $10^{-1}$ and spacing between the cylinders was less than 10 diameters. In their words, at sufficiently low $Re_c$ and tight spacing, the row of cylinders behaved as a paddle rather than a rake. Based on this result, we anticipate that if roughness elements were cylindrical (i.e. hairs or fibrous elements) and were spaced sufficiently closely, then the flow would be excluded between the roughness. Under this condition $d_e > d_c + 2\varepsilon$ and overall capture to the cylinder could be reduced, as depicted in Figure 3-11B. Further investigation should be carried out to describe the drag created by roughness elements and to determine more accurately how increasing roughness density causes a transition from enhanced capture to diminished capture.

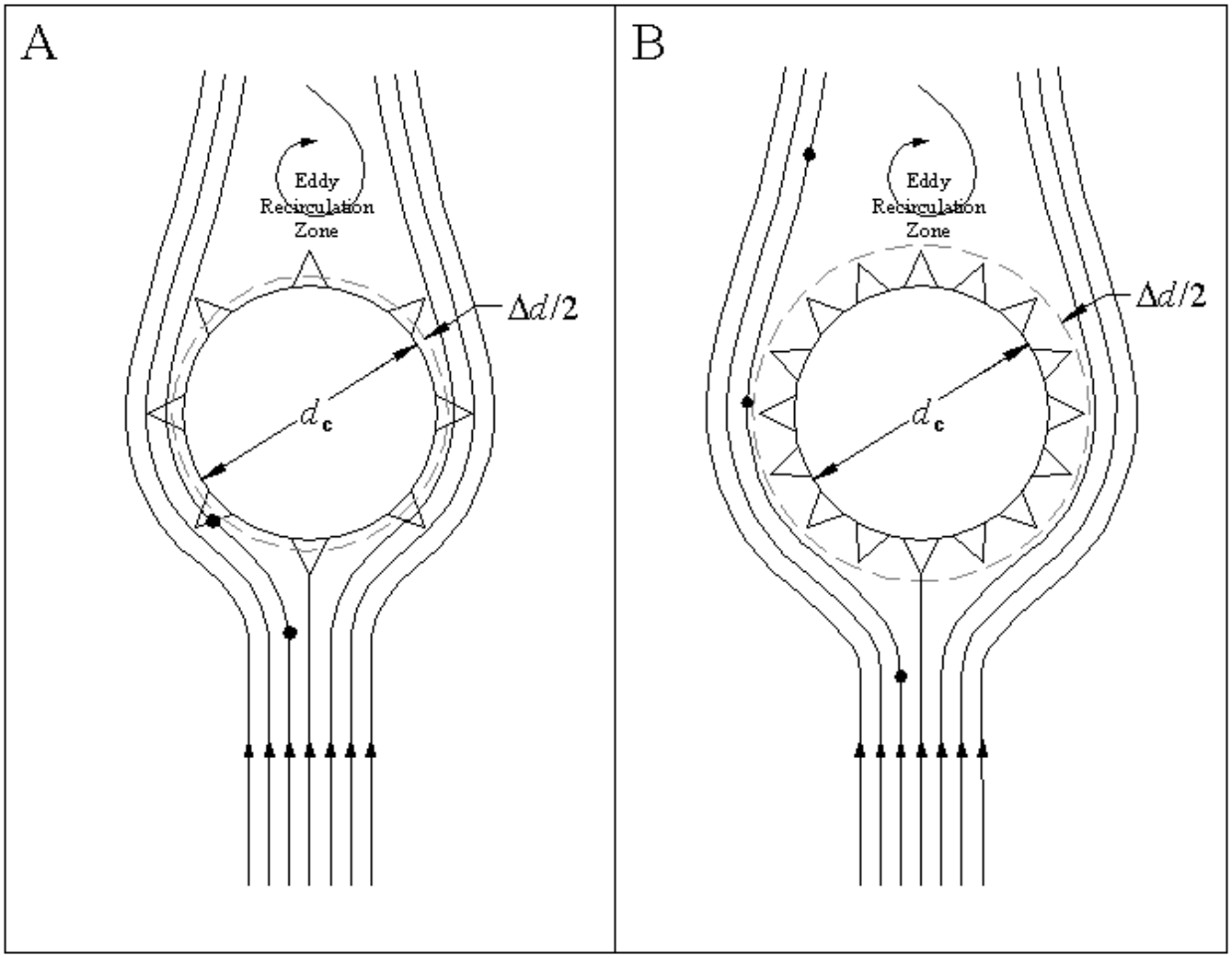


Figure 3-11. Streamlines around rough cylinders. (A) The additional drag created by the roughness elements creates a small change in diameter, $\Delta d$. The effective diameter, $d_c + \Delta d$, is not much larger than the real diameter, $d_c$, such that the additional drag doesn't significantly alter the flow field. Streamlines pass between the roughness elements, which enhance capture due to their high efficiencies. (B) The additional drag is significant enough that streamlines are pushed beyond the roughness elements. Particles depositing via direct interception do not reach the roughness elements and overall capture efficiency of the cylinder is diminished.

### 3.6 Conclusion

Particle capture by individual, cylindrically-shaped structures at $Re_c$ of 50-500 is shown to vary positively with both $R$ and $Re_c$, but to a lesser extent with the latter. The capture in this $Re_c$ range cannot be predicted by solutions from creeping or potential flow theory, but here are shown to follow an empirical power-law function of $R$ and $Re_c$. Further, the empirical relationship is consistent with published values for complex structures composed of cylindrical branches, indicating that these results can also be applied to more complex shapes. Finally, we found that moderate levels of roughness on the

cylinder enhance particle capture for all comparisons, but we believe that excessive roughness may reduce capture efficiencies.

# Chapter 4
# Model of Particle Removal in a Typical Wetland

For many years people have noted that wetlands can improve water quality, namely through the process of particle settling. As discussed in section 1.1, though, particle capture by vegetation has been indicated as an additional mechanism by which wetlands reduce suspended sediment concentration. To quantify the potential importance of this mechanism, a model is developed that accounts for capture to stems as well as gravitational settling in a typical emergent *Spartina alterniflora* coastal wetland.

### 4.1 Model Description

For a wetland of some length, $L_w$, and unit width, (1.12) can be rewritten in a per-unit-volume form, where $V$ is volume of water:

$$\frac{1}{V}\frac{dN_c}{dt} = \frac{\eta P u d_c l_c}{V} = \eta P u d_c l_c'. \tag{4.1}$$

$N_c/V$ is equal to $P$. The total collector length per unit volume, $l_c'$, is defined as $l_c/V$. Whereas before this equation described accumulation to a single collector, now (4.1) describes the number of particles removed per volume per time in the wetland system. Additionally, particles are lost from the water column through settling. A settling model identical to (3.9) is employed in which turbulence is assumed

to keep the concentration vertically uniform, so that loss due to settling is first order. The total rate of change of particle concentration in the wetland is then:

$$\frac{dP}{dt} = -\eta P u d_c l_c' - \frac{w_s}{h} P \tag{4.2}$$

$K_C$ and $K_S$ are the rate constants for capture and settling, respectively, and are defined as $K_C = \eta u d_c l_c'$ and $K_S = w_s/h$. Finally, after integration, the solution for concentration in the water column is:

$$\frac{P}{P_0} = \exp\left(-\left(K_c + K_S\right)t\right) \tag{4.3}$$

To examine the importance of particle capture in a wetland, the removal by the combined mechanisms of capture and settling is compared to the removal achieved by settling alone. $L_{50}$ is defined as the length of wetland required for the concentration of particles to be reduced by 50%. In (4.3) $t = L/u$ and:

$$L_{50} = 0.693\left(\frac{u}{K_C + K_S}\right) \tag{4.4}$$

For settling alone, $K_c$ is set to zero in (3.19).

**4.2 Wetland Model Parameters**

Physical parameters for the model, shown in Table 4-1, were chosen based on typical values observed in real wetlands (e.g. Valiela et al. 1978), with the constraint that $Re_c$ and $R$ be appropriate for use with (3.15). Two representative particle diameters, 50 μm and 300 μm, were used, as well as three flow velocities of 1, 5, and 10 cm $s^{-1}$. Although larger and smaller values of $d_p$ and $u$ might be observed in wetlands, the chosen values give $R$= 0.006 - 0.6 and $Re_c$= 6-1000, ranges over which (3.15) is shown to be valid.

*S. alterniflora* has two forms, called short and tall, the primary difference being that the stem diameter and height are smaller in the short form. Areal stem density, stem height, and histograms of

stem diameter as reported by Valiela et al. (1978) were used to compute $d_c$ and $l_c$'. Histograms of stem diameters from Valiela et al. (1978) are shown in Figure 4-1. The branches of *S. alterniflora* also contribute to capture. These were accounted for by assuming that branch diameter is one-half of stem diameter, and that submerged branch length is one-third of the submerged stem height. For each bin of stem diameters given in the histogram (Valiela et al 1978), $R$ and $Re_c$ were computed, allowing $\eta$ to be found from (3.15). $K_C$ was then computed for each bin of diameters. The total rate constant is simply the sum of the values for each bin.

The settling velocity, $w_s$ ,was computed using standard equations for terminal velocity of a settling sphere (see e.g. Streeter and Wylie 1985). By summing the weight, buoyancy and drag forces around a sphere in a fluid, one obtains the equation for the terminal velocity of a sphere:

$$w_s = \sqrt{\frac{4}{3}\frac{g(\rho_p - \rho)d_p}{\rho C_D}} \tag{4.5}$$

where $g$ is gravity, $\rho_p$ is the density of the particle, $\rho$ is density of the fluid, $d_p$ is the particle diameter, and $C_D$ is the drag coefficient of the sphere for the corresponding Reynolds number of $Re = w_s\, d_p/\nu$. For creeping flow (meaning $Re<1$), $C_D=24/Re$, and $w_s$ is easily solved for as:

$$w_s = \frac{g(\rho_p - \rho)d_p^2}{18\mu} \tag{4.5}$$

For higher Reynolds number flows, the empirical approximation for $C_D$ must be used and the process of solving for $w_s$ is iterative. For $1<\mathrm{Re}<10^4$, $C_D$ can be approximated as:

$$C_D = \frac{24}{Re} + \frac{3}{\sqrt{Re}} + 0.34 \tag{4.7}$$

The height, $h$, of water in the wetland was taken to be 15 cm, and all the vegetation was assumed to be emergent (i.e. stem height > 15 cm). $L_{50}$ was then calculated from (4.4) for particle removal by settling and filtration combined. For comparison, $L_{50}$ contributed by settling alone was calculated from (4.4) with $K_c = 0$.

Table 4-1. Parameters for wetland removal model. Wetland vegetation was modeled from stand characteristics of short form and tall form *Spartina alterniflora* reported by Valiela et al. (1978). $d_p$, $d_c$, and $u$ were chosen so that $Re_c$ and $R$ met the requirements of (3.15).

| | Short Form | Tall Form |
|---|---|---|
| $Re_c$ | 6 - 300 | 10 - 1000 |
| $R$ | 0.02 - 0.6 | 0.006 - 0.15 |
| $u$ | 1, 5, 10 cm $s^{-1}$ | 1, 5, 10 cm $s^{-1}$ |
| $d_p$ | 50, 300 μm | 50, 300 μm |
| $d_c$ | 0.5 - 3 mm | 2 - 9 mm |

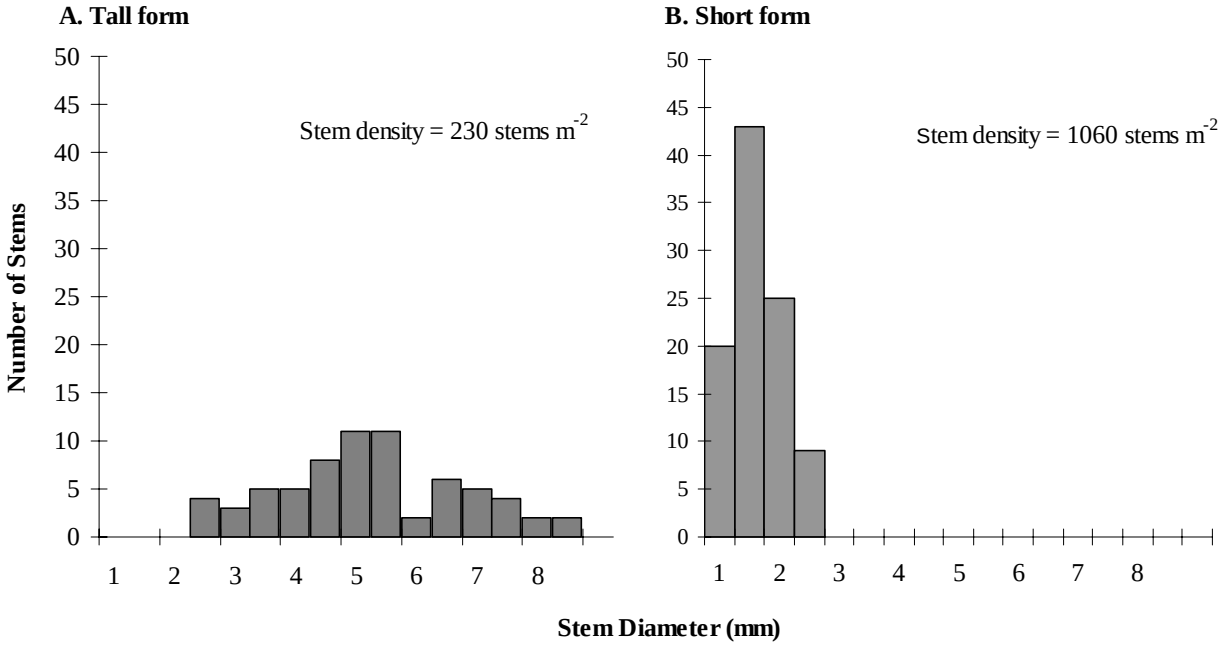


Figure 4-1. Distribution of *Spartina alterniflora* stem diameters per square meter from Valiela et al. (1978). In general tall form S. alterniflora has larger diameters and is less dense than short form.

## 4.3 Results

$L_{50}$ is plotted against the depth-averaged velocity in Figure 4-2. For both particle sizes, removal by particle capture is significant for $u \geq 3$ cm $s^{-1}$. Above this, the rate of removal due to particle capture is

the order of magnitude of or greater than the rate of removal due to settling. In general the decrease in $L_{50}$ is more significant for the short form, reflecting both the higher stem density typical of this form, as well as the strong dependence of capture efficiency with particle ratio, *R*. The short form has the smaller stem and branch diameters and thus larger *R*. This example indicates that particle capture can contribute significantly to the removal of light particles and pathogens, i.e. with $s$ = 1.03, as considered here.

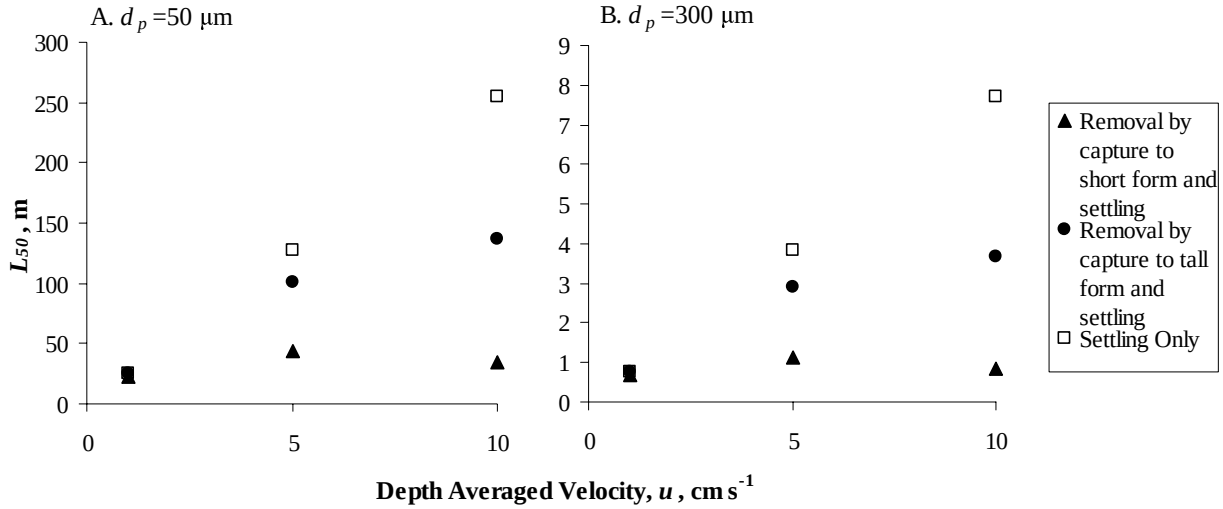


Figure 4-2. Particle removal due to vegetation filtration and settling in a typical wetland. $L_{50}$ is the length of wetland necessary to reduce the initial concentration by 50%, due either to settling alone (the base case) or to the combination of settling and vegetation filtration. Above $u$=3 cm s$^{-1}$, capture to both short and tall form *Spartina alterniflora* becomes a significant mechanism of particle removal.

# Chapter 5
# Conclusions and Future Research

## 5.1 Conclusions

Due to a lack of quantitative information on particle capture efficiency in aquatic flow regimes, experiments are conducted to measure capture efficiency, $\eta$, of a single cylindrical collector over $Re_c$=50-500 and $R$=0.008 – 0.016. Results show that $\eta$ is dependent on $Re_c$ and $R$, but more strongly so on $R$. In an aquatic system with a fixed particle type and size, the amount of particle capture will be most strongly influenced by collector diameter, with the smallest collectors (which have the largest R values) collecting proportionally more particles.

Results from the single-cylinder capture experiments lead to an empirical equation that predicts capture efficiency as a power law function of $Re_c$ and $R$. The empirical equation predicts observed single-cylinder capture efficiencies to within 10% of the observed value. Additionally, published particle capture observations of larval settlement to branched structures (Harvey et al. 1995) are predicted by the empirical equation, indicating that single-cylinder capture efficiencies can be used to predict capture efficiencies of composite cylindrical structures.

Finally, single-cylinder capture experiments with roughness added to the collectors show that roughness increases particle capture efficiency when compared to smooth capture. It is hypothesized, however, that high densities of roughness elements will tend to reduce capture. Although this scenario of

roughness is not achieved with conically-shaped roughness elements, cylindrical roughness elements may lead to this conditon. An argument based on the drag of these elements is presented and criteria are given for when excess drag due to roughness may decrease particle capture efficiency.

### 5.2 Future Research

This study examined capture efficiency of single cylinders and was able to show that in the case of one published data set, single cylinder efficiencies could be applied to structures consisting of more complex arrangements of cylinders. Further investigation should be carried out to see how the capture efficiencies of other natural structures compare to that of single cylinders. In other words, what are the limitations of applying single-cylinder capture efficiencies to composite structures?

An obvious extension of this research is to begin looking at how actual wetland plants capture particles. In this study, each particle that encounters a collector was assumed to be captured. However, the periphyton layers of real wetland stems may not behave as the grease did on the collectors used in these experiments. Thus, future research should be done on how "sticky" periphyton layers are and how this influences capture. For example, suppose *Spartina alterniflora* stems are shown to capture 80% of particles that encounter them. This species would then have a "stickiness factor" of 0.8. This factor could be applied to the efficiencies predicted by the empirical equation (3.15) in order to quantify the number of particles retained on the plant stem.

One question this research attempts to answer, but does not do so fully, is "how much roughness is too much?" That is, at what density of roughness on a collector's surface does particle capture efficiency become diminished? Conical roughness elements were examined here, but were not able to provide enough roughness to reach this condition. As has been hypothesized in section 3.5, cylindrical roughness may increase the drag of the cylinder, pushing streamlines outward and reducing capture efficiency. Further study should be conducted on how cylindrical roughness elements, in high density, may lead to reduced particle capture.

# References


Ackerman, J. D. 1995. Convergence of filiform pollen morphologies in seagrasses - functional mechanisms. Evol. Ecol. **9**: 139-153.

Beckett, K. P., P. H. Freer-Smith, and G. Taylor. 1998. Urban woodlands: Their role in reducing the effects of particulate pollution. Environ. Pollut. **99**: 347-360.

Borowitzka, M. A., and R. C. Lethbridge. 1989. Seagrass epiphytes, p. 458-498. *In* A. W. D. Larkum, A. J. McComb and S. A. Shepherd, [eds.]. Biology of seagrasses. Elsevier.

Butman, C. A. 1987. Larval settlement of soft-sediment invertebrates - the spatial scales of pattern explained by active habitat selection and the emerging role of hydrodynamical processes. Oceanogr. Mar. Biol. **25**: 113-165.

Cheer, A. Y. L., and M. A. R. Koehl. 1987. Paddles and rakes: Fluid flow through bristled appendages of small organisms. Journal of Theoretical Biology **129**: 17-39.

Chen, Y. C. 1955. Filtration of aerosols by fibrous media. Chem. Rev. **55**: 595-623.

Eckman, J. E. 1983. Hydrodynamic processes affecting benthic recruitment. Limnol. Oceanogr. **28**: 241-257.

Elimelech, M., J. Gregory, X. Jia, and R. A. Williams. 1995. Particle deposition and aggregation: Measurement, modelling and simulation, *Colloid and surface engineering series*. Butterworth-Heinemann.

Elliott, A. H. 2000. Settling of fine sediment in a channel with emergent vegetation. Journal of Hydraulic Engineering **126**: 570-577.

Fuchs, N. A. 1964. The mechanisms of aerosols. Pergamon Press Ltd.

Gacia, E., T. C. Granata, and C. M. Duarte. 1999. An approach to measurement of particle flux and sediment retention within seagrass (*Posidonia oceanica*) meadows. Aquatic Botany **65**: 255-268.

Guarraci, M. 1999. Interaction between epiphyte biomass and resuspended inorganic materials on leaves of natural and artificial submersed vegetation. *MS thesis*. University of Maryland at College Park.

Harvey, M., E. Bourget, and R. G. Ingram. 1995. Experimental evidence of passive accumulation of marine bivalve larvae on filamentous epibenthic structures. Limnol. Oceanogr. **40**: 94-104.

Hoerner, S. F. 1965. Fluid dynamic drag: Practical information on aerodynamic drag and hydrodynamic resistance. Hoerner Fluid Dynamics.

Hosokawa, Y., and T. Horie. 1992. Flow and particulate nutrient removal by wetlands with emergent macrophytes, p. 1271-1282. *In* R. Vollenweider, R. Marchetti and R. Viviani, [eds.]. Marine coastal eutrophication: Science of the total environment. Elsevier.

Hotchkiss, N. 1972. Common marsh, underwater & floating-leaved plants of the United States and Canada. Dover.

Johnstone, H. F., and M. H. Roberts. 1949. Deposition of aerosol particles from moving gas streams. Industrial and Engineering Chemistry **41**: 2417-2423.

Jordan, T., J. Pierce, and D. Correll. 1986. Flux of particulate matter in the tidal marsh and subtidal shallows of the Rhode River estuary. Estuaries **9**: 310-319.

Knight, R. L., R. H. Kadlec, and H. M. Ohlendorf. 1999. The use of treatment wetlands for petroleum industry effluents. Environ. Sci. Technol. **33**: 973-980.

Koehl, M. A. R. 1996. When does morphology matter. Annual Review of Ecology and Systematics **27**: 501-524.

Lamb, H. 1932. Hydrodynamics. 6th ed. The University Press.

Langmuir, I. 1942. Filtration of aerosols and the development of filter materials: Office of Scientific Research and Development. Report No. 865.

Langmuir, I., and K. Blodgett. 1946. A mathematical investigation of water droplet trajectories. Washington, D.C.: U.S. Army Air Forces Technical Report No. 5418.

Leonard, L. A., A. C. Hine, and M. E. Luther. 1995. Surficial sediment transport and deposition processes in a *Juncus-roemerianus* marsh, west-central Florida. J. Coast. Res. **11**: 322-336.

Lopez, F., and M. Garcia. 1998. Open-channel flow through simulated vegetation: Suspended sediment transport modeling. Water Resour. Res. **34**: 2341-2352.

Natanson, G. L. 1957. Diffusive deposition of aerosols on a cylinder in a flow in the case of small capture coefficients. Dokl. Akad. Nauk SSSR **112**: 100-103.

Paterson, D. M., and K. S. Black. 1999. Water flow, sediment dynamics and benthic biology. Advances in Ecological Research **29**: 155-193.

Pettersson, T. J. R., H. M. Nepf, and J. D. Ackerman. In Prep. Modeling the deposition of particles on reed-like aquatic vegetation.

Ranz, W. E. 1951. Impaction of aerosol particles on cylindrical and spherical collectors: Technical Report No. 3, Serial No. S0-004. University of Illinois.

Raudkivi, R. J. 1998. Loose boundary hydraulics, 4th ed. Balkema.

Reay, P. 1972. The accumulation of arsenic from arsenic-rich natural water by aquatic plants. J. Applied Ecology **9**: 557-565.

Riisgard, H. U., and P. S. Larsen. 2001. Minireview: Ciliary filter feeding and bio-fluid mechanics - present understanding and unsolved problems. Limnol. Oceanogr. **46**: 882-891.

Rubenstein, D. I., and M. A. R. Koehl. 1977. The mechanicsms of filter feeding: Some theoretical considerations. American Naturalist **111**: 981-994.

Sansalone, J. J., and S. G. Buchberger. 1997. Characterization of solid and metal element distributions in urban highway stormwater. Water Sci. Technol. **36**: 155-160.

Shimeta, J., and P. A. Jumars. 1991. Physical mechanisms and rates of particle capture by suspension feeders. Oceanogr. Mar. Biol. Annu. Rev. **29**: 191-257.

Sin, V. K., and R. M. C. So. 1987. Local force measurements on finite-span cylinders in a cross-flow. Journal of Fluids Engineering - Transactions of the ASME **109**: 136-143.

Sontek. 1997. Sontek doppler current meters – using signal strength data to monitor suspended sediment concentration. San Diego: Sontek.

Spielman, L. A. 1977. Particle capture from low-speed laminar flows. Am. Rev. Fluid Mech. **9**: 297-319.

Streeter, V., and E. B. Wylie. 1985. Fluid mechanics. 8th ed. McGraw-Hill Book Company.

Stumpf, R. P. 1983. The process of sedimentation on the surface of a salt marsh. Estuarine, Coastal and Shelf Science **17**: 495-508.

Taylor, J. R. 1997. An introduction to error analysis: The study of uncertainties in physical measurements. University Science Books.

Vaithiyanathan, P., A. Ramanathan, and V. Subramanian. 1993. Transport and distribution of heavy-metals in Cauvery River. Water Air Soil Pollut. **71**: 13-28.

Valiela, I., J. M. Teal, and W. G. Deuser. 1978. The nature of growth forms in the salt marsh grass *Spartina alterniflora*. American Naturalist **112**: 461-470.

Wetzel, R. G. 2001. Limnology, lake and river ecosystems, 3rd ed. Academic.

Wildish, D., and D. Kristmanson. 1997. Benthic suspension feeders and flow. The University Press.